



**HAL**  
open science

## Diffusion posterior sampling for simulation-based inference in tall data settings

Julia Linhart, Gabriel Victorino Cardoso, Alexandre Gramfort, Sylvain Le Corff, Pedro Luiz Coelho Rodrigues

► **To cite this version:**

Julia Linhart, Gabriel Victorino Cardoso, Alexandre Gramfort, Sylvain Le Corff, Pedro Luiz Coelho Rodrigues. Diffusion posterior sampling for simulation-based inference in tall data settings. 2024. hal-04459545v1

**HAL Id: hal-04459545**

**<https://hal.science/hal-04459545v1>**

Preprint submitted on 15 Feb 2024 (v1), last revised 11 Apr 2024 (v2)

**HAL** is a multi-disciplinary open access archive for the deposit and dissemination of scientific research documents, whether they are published or not. The documents may come from teaching and research institutions in France or abroad, or from public or private research centers.

L'archive ouverte pluridisciplinaire **HAL**, est destinée au dépôt et à la diffusion de documents scientifiques de niveau recherche, publiés ou non, émanant des établissements d'enseignement et de recherche français ou étrangers, des laboratoires publics ou privés.



Distributed under a Creative Commons Attribution 4.0 International License

# Diffusion posterior sampling for simulation-based inference in tall data settings

Julia Linhart<sup>‡</sup>, Gabriel Victorino Cardoso<sup>\*</sup>, Alexandre Gramfort<sup>‡</sup>, Sylvain Le Corff<sup>†</sup>, and  
Pedro L. C. Rodrigues<sup>II</sup>

<sup>‡</sup>Université Paris-Saclay, Inria, CEA.

<sup>\*</sup>CMAP, École Polytechnique, Institut Polytechnique de Paris.

<sup>†</sup>LPSM, Sorbonne Université, UMR CNRS 8001.

<sup>II</sup>Univ. Grenoble Alpes, Inria, CNRS, Grenoble INP, LJK.

## Abstract

Determining which parameters of a non-linear model could best describe a set of experimental data is a fundamental problem in Science and it has gained much traction lately with the rise of complex large-scale simulators (a.k.a. *black-box* simulators). The likelihood of such models is typically intractable, which is why classical MCMC methods can not be used. Simulation-based inference (SBI) stands out in this context by only requiring a dataset of simulations to train deep generative models capable of approximating the posterior distribution that relates input parameters to a given observation. In this work, we consider a *tall data* extension in which multiple observations are available and one wishes to leverage their shared information to better infer the parameters of the model. The method we propose is built upon recent developments from the flourishing score-based diffusion literature and allows us to estimate the *tall data* posterior distribution simply using information from the score network trained on individual observations. We compare our method to recently proposed competing approaches on various numerical experiments and demonstrate its superiority in terms of numerical stability and computational cost.

## 1 Introduction

Inverting non-linear models describing natural phenomena is a fundamental problem in Science and has been tackled by many fields Gonçalves et al. (2020); Vasist et al. (2023); Dax et al. (2023). In this work, we consider a Bayesian approach Tarantola (2005) in which the input parameters  $\theta \in \mathbb{R}^m$  of a model  $\mathcal{M}$  that best explain a set of output observations  $x \in \mathbb{R}^d$  are described via a posterior distribution  $p(\theta | x)$ . Obtaining samples of the posterior can, however, be very challenging when the outputs of  $\mathcal{M}$  are obtained through complex simulations (e.g. solutions of non-linear differential equations Jansen and Rit (1995)). Indeed, in these cases the likelihood function  $p(x | \theta)$  is often impossible to evaluate and MCMC procedures can not be used.

Simulation-based inference (SBI) Cranmer et al. (2020) is a promising approach that bypasses the difficulties of likelihood evaluations via simulations from the model and leverages the recent advances from deep generative learning. The procedure relies on the choice of a prior distribution  $\lambda(\theta)$  encoding knowledge

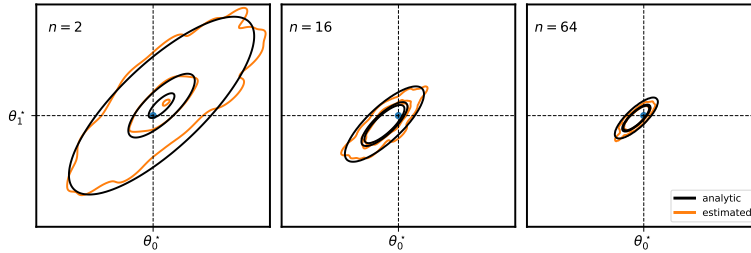


Figure 1: The posterior distribution of a Gaussian simulator model with Gaussian prior concentrates around the **true parameter**  $\theta^*$  as the number  $n$  of observations  $x_i^* \sim p(x | \theta^*)$  increases. We compare the **analytic** posterior to the posterior **estimated** with our score-based proposal (GAUSS).

about the values of  $\mathcal{M}$ 's parameters and a simulated dataset generated as per:

$$\Theta_i \sim \lambda(\theta), \quad X_i \sim p(x | \Theta_i), \quad (\Theta_i, X_i) \sim p(\theta, x).$$

Letting  $N_s$  be a fixed simulation budget, one can build a dataset  $\mathcal{D} = \{(\Theta_i, X_i)\}_{i=1}^{N_s}$  and train conditional deep generative models to generate samples from  $p(\theta | x^*)$  for any new observation  $x^*$ . Usual approaches approximate either directly the posterior distribution (NPE) Greenberg et al. (2019), the likelihood function (NLE) Papamakarios et al. (2019), or the ratio of likelihoods (NRE) Hermans et al. (2020). In NPE, the posterior samples can be obtained directly by sampling a conditional normalizing flow Papamakarios et al. (2021), whereas in NLE and NRE it is necessary to use a MCMC sampler.

In this work, we consider a natural extension of the above Bayesian framework to a *tall data* setting Bardenet et al. (2015), in which multiple observations  $x_{1:n}^* = (x_1, \dots, x_n)$  are available and the posterior distribution

$$p(\theta | x_{1:n}^*) \propto \lambda(\theta)^{1-n} \prod_{j=1}^n p(\theta | x_j^*), \quad (1)$$

is expected to provide more precise information about how to invert  $\mathcal{M}$  (see Fig 1). Despite being a setup with much practical interest, there has not been many previous works providing a satisfactory extension to usual SBI procedures. In Rodrigues et al. (2021) the authors merge a fixed number of extra observations via a deepset Zaheer et al. (2017) and fall back to NPE with an augmented training dataset with samples  $\mathcal{D}_n = \{(\Theta_i, X_{i,1:n})\}$ . Important drawbacks of such approach are the lack of flexibility on the number of extra observations at inference time and the potentially heavy cost of generating extra observations from the simulator. In Hermans et al. (2020), the authors show how to handle the *tall data* setting with NRE and an equivalent extension can be done for NLE as well Geffner et al. (2023). Note, however, that both approaches still require a MCMC sampler to obtain posterior samples, which is often undesirable in SBI applications.

Recently, Sharrock et al. (2022) proposed to use score-based generative models (SBGM) Ho et al. (2020); Song et al. (2021b) to approximate the conditional posterior distribution targeted in SBI, called *Neural Posterior Score estimation* (NPSE). SBGM introduces an easy to train objective for learning the *score* of a sequence of noisy version of the distribution of the interest via a network  $s_\phi(\theta, x_i, t)$  using the simulated dataset  $\mathcal{D}$ . SBGM rivals state-of-the-art generative models such as generative adversarial networks (GANs) Goodfellow et al. (2014) and normalizing flows in high-dimension challenging datasets without the need of adversarial training or special network architectures.

However, extending NPSE to a *tall data* setting is challenging, as a direct application of the method would require training a score network  $s_\phi(\theta, x_{1:n}, t)$  to approximate  $\nabla_\theta \log p_t(\theta | x_{1:n})$  on an augmented dataset  $\mathcal{D}_n$ , leading to the same drawbacks from the augmented NPE approach. Recently, Geffner et al. (2023) proposed a method named F-NPSE in which an annealed Langevin procedure is used to target the

tall posterior with a sequence of laws from which the score can be computed using the individual scores  $s_\phi(\theta, x_i, t)$ , thus avoiding the requirement of an augmented training dataset. The major drawback of this approach, however, is reintroducing the need of MCMC for sampling from the posterior.

In this paper, we propose an algorithm that approximates the score of the SBGM associated with the *tall data* posteriors using only the individual scores from the individual SBGMs and without a Langevin sampler. We demonstrate the superiority of our approach as compared to F-NSPE on several numerical experiments: two Gaussian toy models for which all quantities of interest are known analytically, three examples from the SBI benchmark Lueckmann et al. (2021a), and the inversion of a challenging model from neuroscience Jansen and Rit (1995).

## 2 Background

### 2.1 Score based generative models (SBGM)

**Score estimation.** The goal of score-based generative modelling is to learn how to sample new data from a target distribution  $q_{\text{data}}$  using an approximation of the score on “noisy versions” of samples from  $q_{\text{data}}$ . In the variance preserving (VP) framework Ho et al. (2020); Yang et al. (2023), a sequence of noisy versions  $\{\theta_t\}_{t \in [1:T]}$  of  $q_{\text{data}}$  is defined for  $t \in [1:T]$ , by

$$\theta_t = \sqrt{\alpha_t} \theta_0 + \sqrt{v_t} \epsilon_t,$$

where  $\theta_0 \sim q_{\text{data}}$ ,  $\{\epsilon_t\}_{t \in [1:T]}$  are i.i.d. with distribution  $\mathcal{N}(0, \text{Id})$ ,  $\{\alpha_t\}_{t \in [1:T]} \in [0, 1]^T$  is a decreasing sequence of positive real numbers and  $v_t = 1 - \alpha_t$ . Let  $q_{t|0}(\theta_t | \theta_0) = \mathcal{N}(\theta_t; \sqrt{\alpha_t} \theta_0, v_t \text{Id})$  be the probability density function of the conditional distribution of  $\theta_t$  given  $\theta_0$  and  $q_t$  the density of  $\theta_t$ . Following the seminal works of Hyvärinen and Dayan (2005); Vincent (2011), we can learn the score of  $q_t$  via a neural network  $s_\psi$  by minimising  $\mathcal{L} : \psi \mapsto \mathbb{E}_{\theta_t \sim q_t} [\|s_\psi(\theta_t, v_t) - \nabla \log q_t(\theta_t)\|^2]$  without knowledge of the ground-truth data score. Using Fisher’s identity, we can define the SBGM loss as

$$\mathcal{L}_{\text{score}}(\psi) = \sum_{t=1}^T \gamma_t^2 \mathbb{E}_{\theta_0 \sim q_{\text{data}}, \theta_t \sim q_{t|0}(\cdot | \theta_0)} [\|s_\psi(\theta_t, v_t) - \nabla \log q_{t|0}(\theta_t | \theta_0)\|^2], \quad (2)$$

where  $\gamma_t$  is a positive weighting function introduced in Vincent (2011).

**Backward sampling.** Once we have the score approximation  $s_\psi(\theta_t, v_t)$  of  $\nabla \log q_t(\theta_t)$ , our goal is to sample *backwards* from the distributions  $q_T, \dots, q_1$ . There are many ways of carrying out this sampling, such as using annealed Langevin dynamics Song and Ermon (2019), stochastic differential equations Song et al. (2021b), or ordinary differential equations Karras et al. (2022). In this work, we follow the approach proposed in Song et al. (2021a), which yields the denoising diffusion implicit models (DDIM) sampler. DDIM introduces a set inference distributions indexed by  $\sigma = \{\sigma_t \in (0, \alpha_{t-1}^{1/2})\}_{t \in [1:T-1]}$  defined for  $t \in [1:T-1]$  as:

$$q_{t|t+1,0}^\sigma(\theta_t | \theta_0, \theta_{t+1}) = \mathcal{N}(\theta_{t-1}; \mu_t(\theta_0, \theta_t), \sigma_t^2 \text{Id}),$$

with  $\mu_t(\theta_0, \theta_t) = \alpha_{t-1}^{1/2} \theta_0 + (v_{t-1} - \sigma_t^2)^{1/2} (\theta_t - \alpha_t^{1/2} \theta_0) / v_t^{1/2}$ . Note that  $\mu_t$  is chosen so that  $q_{t|0}^\sigma(\theta_t | \theta_0) = \mathcal{N}(\theta_t; \sqrt{\alpha_t} \theta_0, v_t \text{Id})$  (Song et al., 2021a, Lemma 1, Appendix B). This property allows us to write

$$q_{t-1}(\theta_{t-1}) = \int q_{t-1|t,0}^\sigma(\theta_{t-1} | \theta_t, \theta_0) \times q_{0|t}(\theta_0 | \theta_t) q_t(\theta_t) d\theta_0 d\theta_t.$$

Even though the equation above suggests a way of passing from  $q_t$  to  $q_{t-1}$  it involves an intractable kernel  $\int q_{t-1|t,0}^\sigma(\theta_{t-1}|\theta_t, \theta_0)q_{0|t}(\theta_0|\theta_t)d\theta_0$ . The marginal distribution can be approximated by

$$\hat{q}_{t-1}(\theta_{t-1}) = \int q_{t-1|t,0}^\sigma(\theta_{t-1}|\theta_t, \mu_t(\theta_t))q_t(\theta_t)d\theta_t, \quad (3)$$

where  $\mu_t(\theta_t)$  is the conditional mean of  $\theta_0$  given  $\theta_t$  under the inference distribution; i.e  $\mu_t(\theta_t) := \mathbb{E}_{\theta_0 \sim q_{0|t}^\sigma(\cdot|\theta_t)}[\theta_0]$ . As  $\mu_t(\theta_t)$  is not available explicitly, in order to effectively sample from (3), we can estimate  $\mu_t(\theta_t)$  using the approximate score  $s_\psi(\theta_t, t)$ . By noting that

$$\alpha_t^{1/2} \mu_t(\theta_t) - \theta_t = v_t \mathbb{E}_{\theta_0 \sim q_{0|t}^\sigma(\cdot|\theta_t)} [\nabla \log q_{t|0}(\theta_t|\theta_0)],$$

we can use (2) to define the following approximation for all  $t \in [1 : T]$

$$\mu_{\psi,t}(\theta_t) := \alpha_t^{1/2} [\theta_t + v_t s_\psi(\theta_t, v_t)]. \quad (4)$$

We can finally define the backward Markov chain

$$p_{\psi,0:T}(\theta_{0:T}) = p_T(\theta_T) \prod_{t=1}^T p_{\psi,t-1|t}(\theta_{t-1}|\theta_t), \quad (5)$$

where  $p_T(\theta_T) = q_T(\theta_T)$ ,  $p_{\psi,t-1|t}(\theta_{t-1}|\theta_t) = q_{t-1|t,0}^\sigma(\theta_{t-1}|\theta_t, \mu_{\psi,t}(\theta_t))$ , and  $p_{\psi,0|1}(\theta_0|\theta_1) = \mathcal{N}(\theta_0; \mu_{\psi,1}(\theta_1), \sigma_0^2 \text{Id})$ , with  $\sigma_0 > 0$  a free parameter.

Note that we use the procedure described above to learn the score of the conditional distribution of  $\theta$  given  $x$ . To do so, we learn an amortized score  $s_\psi(\theta, x, v_t)$  as in Batzolis et al. (2021).

## 2.2 Factorized neural posterior score estimation

The F-NPSE method proposed in Geffner et al. (2023) defines a sequence of distributions  $\{\varrho_t(\cdot | x)\}_{t \in [0:T]}$  as per

$$\nabla_\theta \log \varrho_t(\theta | x_{1:n}^*) = (1-n)(1-t)\nabla_\theta \log \lambda(\theta) + \sum_{j=1}^n s_\psi(\theta, x_j, v_t), \quad (6)$$

where the score of  $\varrho_0$  is the score of the tall posterior defined in (1) and  $\nabla_\theta \log \lambda(\theta)$  can be computed analytically for common prior choices; see Appendix D. F-NPSE uses Langevin dynamics to sample  $\varrho_t$  for each  $t = T, \dots, 1$  and has shown superior performance as compared to all competing methods for *tall data* settings (i.e. augmented versions of NPE, NLE, and NRE) in terms of posterior reconstruction, achieving the best trade-off between sample efficiency and accumulation of errors when the number of observations grows. However, this performance is at the cost of an increased number of neural net evaluations. The main limitation of F-NPSE is the use of annealed Langevin dynamics which is very sensitive to the choices of step-size at each sampling iteration, as well as the total number of steps.

## 3 Diffusion posterior sampling for tall data

### 3.1 Exact computation of the tall data posterior score

Let  $x_{1:n}^* = \{x_1^*, \dots, x_n^*\} \sim_{\text{iid}} p(x | \theta^*)$  be observations sampled using the same parameter  $\theta^* \in \mathbb{R}^m$ . Our goal is to sample from the *tall data* posterior  $p(\theta | x_{1:n}^*)$  via the backward sampling Markov chain defined

in (5), while only relying on a score estimate  $s_\phi(\theta, x, v_t)$  of  $\nabla_\theta \log p_t(\theta | x)$  of the diffused posterior for a single observation. To do so, we need to build an approximation of the diffused *tall data* posterior score

$$\nabla_{\theta_t} \log p_t(\theta_t | x_{1:n}^*) = \nabla_{\theta_t} \log \int p(\theta | x_{1:n}^*) q_{t|0}(\theta_t | \theta) d\theta$$

that solely depends on  $\nabla_\theta \log p_t(\theta | x_j^*)$ , for all  $j \in [1, n]$ . Using (1) we can write

$$p_t(\theta | x_{1:n}^*) = \int p(\theta_0 | x_{1:n}^*) q_{t|0}(\theta | \theta_0) d\theta_0 \propto \int \left( \lambda(\theta_0)^{1-n} \prod_{j=1}^n p(\theta_0 | x_j^*) \right) q_{t|0}(\theta | \theta_0) d\theta_0. \quad (7)$$

Given the diffused prior  $p_t^\lambda(\theta) = \int \lambda(\theta_0) q_{t|0}(\theta | \theta_0) d\theta_0$ <sup>1</sup>, we now introduce the following backward transition kernels obtained via Bayes' rule:

$$p_{0|t}(\theta_0 | \theta, x) = \frac{p(\theta_0 | x) q_{t|0}(\theta | \theta_0)}{p_t(\theta | x)} \quad (8)$$

$$\text{and } p_{0|t}^\lambda(\theta_0 | \theta) = \frac{\lambda(\theta_0) q_{t|0}(\theta | \theta_0)}{p_t^\lambda(\theta)}. \quad (9)$$

Rearranging terms in equation (7) and replacing them with the quantities in (8), gives us

$$\begin{aligned} p_t(\theta | x_{1:n}^*) &\propto \int (\lambda(\theta_0) q_{t|0}(\theta | \theta_0))^{1-n} \prod_{j=1}^n p(\theta_0 | x_j^*) q_{t|0}(\theta | \theta_0) d\theta_0 \\ &= \int \left( p_{0|t}^\lambda(\theta_0 | \theta) p_t^\lambda(\theta) \right)^{1-n} \prod_{j=1}^n p_{0|t}(\theta_0 | \theta, x_j^*) p_t(\theta | x_j^*) d\theta_0 \\ &= \left( p_t^\lambda(\theta)^{1-n} \prod_{j=1}^n p_t(\theta | x_j^*) \right) L_\lambda(\theta, x_{1:n}^*), \end{aligned}$$

with

$$L_\lambda(\theta, x_{1:n}^*) := \int p_{0|t}^\lambda(\theta_0 | \theta)^{1-n} \prod_{j=1}^n p_{0|t}(\theta_0 | \theta, x_j^*) d\theta_0.$$

The corresponding Fisher score therefore writes

$$\nabla_\theta \log p_t(\theta | x_{1:n}^*) = (1 - n) \nabla_\theta \log p_t^\lambda(\theta) + \sum_{j=1}^n \nabla_\theta \log p_t(\theta | x_j^*) + \nabla_\theta \log L_\lambda(\theta, X_{1:n}^*).$$

The first two terms in the above equation are known: the prior score can be computed analytically in most cases<sup>2</sup> and the (single) posterior scores are approximated by evaluating the learned score model  $s_\phi(\theta, x, v_t)$  in every  $x_j^*$ . This leaves us with the last term, that we still need to approximate.

<sup>1</sup>The diffused prior can be computed analytically for simple cases (e.g. Uniform or Gaussian priors) as in Sharrock et al. (2022).

<sup>2</sup>See Appendix D for the Gaussian and Uniform cases. If not, it can be learned via the classifier-free guidance approach Ho and Salimans (2022), at the same time as the posterior score.

### 3.2 Second order approximation of $\log L_\lambda$

In this section, we consider a Gaussian approximation of the backward kernels defined in (8) via

$$\hat{p}_{0|t}(\theta_0|\theta, x) = \mathcal{N}(\theta_0; \mu_t(\theta, x), \Sigma_t(\theta, x)) \quad (10)$$

$$\text{and } \hat{p}_{0|t}^\lambda(\theta_0|\theta) = \mathcal{N}(\theta_0; \mu_{t,\lambda}(\theta), \Sigma_{t,\lambda}(\theta)), \quad (11)$$

where  $\mu_t(\theta, x)$ ,  $\mu_{t,\lambda}(\theta)$  and  $\Sigma_t(\theta, x)$ ,  $\Sigma_{t,\lambda}(\theta)$  are the means and covariance matrices of the backward processes respectively associated with the diffused posterior  $p_t(\theta | x)$  and prior  $p_t^\lambda(\theta)$  distributions.<sup>3</sup> This leads us to the following estimator of  $\log L_\lambda(\theta, x_{1:n}^*)$ :

$$\ell_\lambda(\theta, x_{1:n}^*) = \log \int \hat{p}_{0|t}^\lambda(\theta_0|\theta)^{1-n} \prod_{j=1}^n \hat{p}_{0|t}(\theta_0|\theta, x_j) d\theta_0. \quad (12)$$

From now on, we alleviate the dependency on  $x_j$  and write  $\mu_{t,j}(\theta) = \mu_{t,j}(\theta, x_j)$  and  $\Sigma_{t,j}(\theta) = \Sigma_t(\theta, x_j)$ . We now state the two Lemmas that are the foundation of our approximation of the score of the tall posterior. All proofs are postponed to Appendix A.

**Lemma 3.1.** *For all  $\theta \in \mathbb{R}^m$ , let  $\Lambda(\theta) = \sum_{j=1}^n \Sigma_{t,j}^{-1}(\theta) + (1-n)\Sigma_{t,\lambda}^{-1}(\theta)$ . Assume that  $\Lambda(\theta)$  is positive definite. Then, for all  $\theta \in \mathbb{R}^m$  and  $x_i^* \in \mathbb{R}^d$ ,  $1 \leq i \leq n$ ,*

$$\ell_\lambda(\theta, x_{1:n}^*) = \sum_{j=1}^n \zeta_j(\theta) + (1-n)\zeta_\lambda(\theta) - \zeta_{\text{all}}(\theta), \quad (13)$$

where

$$\zeta(\mu, \Sigma) = -(m \log 2\pi - \log |\Sigma^{-1}| + \mu^\top \Sigma^{-1} \mu) / 2,$$

and  $\zeta_j(\theta) = \zeta(\mu_{t,j}(\theta), \Sigma_{t,j}(\theta))$  for all  $j \in [1 : n]$ ,  $\zeta_\lambda(\theta) = \zeta(\mu_{t,\lambda}(\theta), \Sigma_{t,\lambda}(\theta))$  and  $\zeta_{\text{all}}(\theta) = \zeta(\Lambda(\theta)^{-1}\eta(\theta), \Lambda(\theta)^{-1})$  with  $\eta(\theta) = \sum_{j=1}^n \Sigma_{t,j}^{-1}(\theta)\mu_{t,j}(\theta) + (1-n)\Sigma_{t,\lambda}^{-1}(\theta)\mu_{t,\lambda}(\theta)$ .

**Lemma 3.2.** *For all  $\theta \in \mathbb{R}^m$  and  $x_i^* \in \mathbb{R}^d$ ,  $1 \leq i \leq n$ , the full gradient can be written as*

$$\begin{aligned} \nabla_\theta \log p_t(\theta | x_{1:n}^*) &= \Lambda(\theta)^{-1} \sum_{j=1}^n \Sigma_{t,j}^{-1}(\theta) \nabla_\theta \log p_t(\theta | x_j) \\ &+ (1-n)\Lambda(\theta)^{-1} \Sigma_{t,\lambda}^{-1}(\theta) \nabla_\theta \log p_t^\lambda(\theta) + F(\theta, x_{1:n}^*), \end{aligned}$$

where  $F(\theta, x_{1:n}^*) = 0$  if  $\nabla_\theta \Sigma_{t,j}(\theta) = 0$  for all  $j \in [1 : n]$  and  $\nabla_\theta \Sigma_{\lambda,t}(\theta) = 0$ .

We now focus on the particular choice of  $\Sigma_{t,i}(\theta)$  that we use in our approximation. It can be shown that  $\Sigma_{t,i}(\theta_t) = \nabla_{\theta_t} \mu_{t,i}(\theta_t)$  Boys et al. (2023). This corresponds to Algorithm 2, which we refer to as JAC. However, this approach possesses two main drawbacks. The first is that it scales poorly with the dimension; indeed, we need to calculate a  $m \times m$  matrix which is prohibitive for large  $m$ . The second is that we have to take the derivative w.r.t. the inputs of the score neural network, which is known to be unstable. Note that as proposed in Boys et al. (2023), we do not propagate gradients through  $\Sigma_{t,i}(\theta_t)$ , rendering  $F(\theta_t, x_{1:n}^*) = 0$  in Lemma 3.2.

<sup>3</sup>Note that  $\mu_t(\theta) = \mathbb{E}[\theta_0 | \theta]$  and  $\Sigma_t(\theta) = \mathbb{E}[(\theta_0 - \mu_t(\theta))(\theta_0 - \mu_t(\theta))^\top | \theta]$ . They are explicitly known for certain distribution choices and are respectively functions of the score and its derivatives; see Boys et al. (2023).

As an alternative, we consider a constant approximation of the covariance matrix. To do so, we start by noting that in the case where  $q_{\text{data}}$  is a Gaussian distribution with mean  $\mu_0$  and variance  $\Sigma_0$ , we have  $\Sigma_t = (\Sigma_0^{-1} + \alpha_t v_t^{-1} \text{Id})^{-1}$ , see Appendix D. Note that choosing  $\Sigma_0 = I_m$  results in the approximation proposed by Song et al. (2023). We use the formula for the Gaussian case as an approximation of the real covariance matrix, yielding Algorithm 1 which we refer to as GAUSS. To do so, we need to first estimate  $\Sigma_0$  for each  $x$ , which we do by first running a DDIM with a small number of iterations (100) for each  $i$  and using the empirical covariance matrix of the samples as  $\Sigma_0$ . Note that in this case, we also have  $F(\theta_t, x_{1:n}) = 0$  in Lemma 3.2.

---

**Algorithm 1** GAUSS (Gaussian approximation)

---

**Input:**  $\theta, x_{1:n}, t, \hat{\Sigma}_{1:n}, \text{prior\_fn}$   
**Output:**  $s_{1:n}$   
 $\Sigma_{t,\lambda}^{-1}, s_\lambda \leftarrow \text{prior\_fn}(\theta, t)$   
**for**  $j \leftarrow 1$  **to**  $n$  **do**  
     $s_j \leftarrow s_\psi(\theta, x_j, v_t)$   
     $\hat{\Sigma}_{t,j}^{-1} \leftarrow \hat{\Sigma}_j^{-1} + \frac{\alpha_t}{v_t} \text{Id}$   
**end for**  
 $\Lambda \leftarrow (1 - n)\Sigma_{t,\lambda}^{-1} + \sum_{i=1}^n \hat{\Sigma}_{t,i}^{-1}$   
 $\tilde{s}_{1:n} \leftarrow (1 - n)\Sigma_{t,\lambda}^{-1} s_\lambda + \sum_{i=1}^n \hat{\Sigma}_{t,i}^{-1} s_i$   
 $s_{1:n} \leftarrow \text{LinSolve}(\Lambda, \tilde{s}_{1:n})$

---



---

**Algorithm 2** JAC (Jacobian approximation)

---

**Input:**  $\theta, x_{1:n}, t, \text{prior\_fn}$   
**Output:**  $s_{1:n}, \Sigma_{t,\lambda}^{-1}, s_\lambda \leftarrow \text{prior\_fn}(\theta, t)$   
**for**  $j \leftarrow 1$  **to**  $n$  **do**  
     $s_j \leftarrow s_\psi(\theta, x_j, v_t)$   
     $\hat{\Sigma}_{t,j}^{-1} \leftarrow \frac{\alpha_t}{v_t} [\text{Id} + v_t \nabla_\theta s_\psi(\theta, x_j, v_t)]^{-1}$   
**end for**  
 $\Lambda \leftarrow (1 - n)\Sigma_{t,\lambda}^{-1} + \sum_{i=1}^n \hat{\Sigma}_{t,i}^{-1}$   
 $\tilde{s}_{1:n} \leftarrow (1 - n)\Sigma_{t,\lambda}^{-1} s_\lambda + \sum_{i=1}^n \hat{\Sigma}_{t,i}^{-1} s_i$   
 $s_{1:n} \leftarrow \text{LinSolve}(\Lambda, \tilde{s}_{1:n})$

---

## 4 Experiments

In this section, we investigate the performance of GAUSS and JAC for different tasks from SBI literature with increasing difficulty. We take F-NPSE Geffner et al. (2023) as baseline for comparisons, which uses unadjusted Langevin dynamics (ULD) with  $L = 5$  steps and  $\tau = 0.5$ . We have decided to not compare our methods to augmented versions of NPE, NLE, and NRE because this has already been done in Sharrock et al. (2022) and Geffner et al. (2023) with the score-diffusion framework demonstrating clearly superior performance. Of course, this choice reduces the range of comparisons of our experimental section, but allows us to focus solely on the best alternative method from current literature. For GAUSS and JAC we sample with the backward Markov chain defined in Section 2 with  $\sigma_t^2 = \eta^2 (v_{t-1}/v_t) (1 - \alpha_t/\alpha_{t-1})$  where  $\eta = 0.2, 0.5, 0.8, 1$  for a number of steps  $T = 50, 150, 400, 1000$  respectively. We use an uniform scheduling  $\{t_i = i/T\}_{i=1}^T$ . The code reproducing all experiments is available in the following repository.<sup>4</sup>

### 4.1 Gaussian toy models

We consider two toy examples for which the analytic form of the posterior and corresponding score distributions are known. Our first example is a multivariate Gaussian simulator  $p(x | \theta) = \mathcal{N}(x; \theta, (1 - \rho)\mathbf{I}_m + \rho\mathbf{1}_m)$  with correlation factor  $\rho = 0.8$ . The second is a Mixture of Gaussians simulator (GMM)  $p(x | \theta) = 0.5\mathcal{N}(x; \theta, 2.25\Sigma) + 0.5\mathcal{N}(x; \theta, \Sigma/9)$ , where  $\Sigma$  is a diagonal matrix with values increasing linearly between 0.6 and 1.4, following Geffner et al. (2023). Both examples are carried out with a Gaussian prior  $\lambda(\theta) = \mathcal{N}(\theta; 0, \mathbf{I}_m)$  in dimension  $m = 10$ . Here, the samples of the true posterior for multiple observations are obtained either directly for Gaussian or via Metropolis Adjusted Langevin (MALA) for

<sup>4</sup><https://anonymous.4open.science/r/diffusions-for-sbi-7675>



GMM (see Appendix E for further details). We use the sliced Wasserstein (sW) distance to measure how close the obtained posterior samples are to the true samples.<sup>5</sup> The sW is computed with  $10^4$  slices, on  $10^3$  samples and results are reported over 5 different seeds. Consider the following approximate score model

$$\tilde{s}_\psi(\theta, x, v_t) = s_\psi(\theta, x, v_t) + \epsilon v_t r(\theta, x, v_t),$$

where  $\epsilon \geq 0$ ,  $s_\psi(\theta, x, v_t)$  is the analytical posterior score and  $r$  is a randomly initialized neural net with outputs in range  $[-1, 1]$ , see Appendix D. This construction leads to an error of  $\epsilon$  over the “noise predictor” network defined as  $-\tilde{s}_\psi(\theta, x, v_t)/v_t$ , which is the neural network that one actually optimizes when training a score model. Note that unlike the Gaussian case, Tweedie’s approximation is not exact for GMM, i.e.  $p_{0|t_1}(\theta_0|\theta_t)$  is not a Gaussian density for all  $\theta_t$  and all  $t \in [1 : T]$ . Therefore, this example allows us to quantify the effect of Tweedie’s approximation while still controlling the score estimation error (through  $\epsilon$ ).

Table 1 displays the total running time and sW for each algorithm on the Gaussian example (Table 3 in Appendix F shows similar results for GMM). Based on this table, we consider “equivalent time settings”, namely we run our algorithm with 400 and 1000 steps for **JAC** and **GAUSS** respectively and **LANGEVIN** for 400 steps. We can see that our algorithm yields smaller sW than the equivalent Langevin sampler while accounting for 5 times less neural network evaluation (NNE), thus 5 times faster. We show in Appendix F the differences in speed for each tested setting.

Algorithm	N steps	$\Delta t$ (s)	sW
GAUSS	50	0.45 +/- 0.00	0.17 +/- 0.08
JAC	50	0.41 +/- 0.00	3.14 +/- 4.12
LANGEVIN	50	0.83 +/- 0.00	nan +/- nan
GAUSS	150	0.90 +/- 0.00	0.17 +/- 0.06
JAC	150	1.22 +/- 0.00	1.57 +/- 2.33
LANGEVIN	150	2.50 +/- 0.01	0.65 +/- 0.42
GAUSS	400	2.04 +/- 0.00	0.20 +/- 0.11
<b>JAC</b>	400	3.26 +/- 0.01	0.85 +/- 1.20
<b>LANGEVIN</b>	400	6.65 +/- 0.02	0.65 +/- 0.43
<b>GAUSS</b>	1000	4.77 +/- 0.01	0.22 +/- 0.10
JAC	1000	8.18 +/- 0.03	0.25 +/- 0.09
LANGEVIN	1000	16.65 +/- 0.03	0.65 +/- 0.42

Table 1: Sliced Wasserstein and total elapsed time for the Gaussian toy example with  $m = 10$ ,  $n = 32$  and  $\epsilon = 10^{-2}$  per algorithm and number of sampling steps. Mean and std over 5 different seeds.

Figure 2 portrays the effect of the perturbation  $\epsilon$  in the posterior approximation for each algorithm for  $n \in [1, 100]$ . In the Gaussian example we see that **GAUSS** is better in all settings. This is the expected behaviour, since in this example our method based on second order approximations fits perfectly the score of the tall posterior. **JAC** is exact for zero or very small perturbations ( $\epsilon = 0, 0.001$ ), but becomes unstable when it increases ( $\epsilon = 0.01$ ). In GMM, our approximation **GAUSS** is competitive with **LANGEVIN**, achieving smaller sW for small  $n$  and then reaching the same sW for  $n = 90$ , while being the best for all  $n$  in the setting with the highest amount of perturbation ( $\epsilon = 10^{-1}$ ). We see that **JAC** is extremely precise for  $\epsilon = 0$  (which corresponds to the case when the analytical posterior score is available) and becomes unstable for  $\epsilon > 0$ . This suggests that **GAUSS** offers a good trade-off between precision and robustness. It is thus the

<sup>5</sup>In order to account for the finite-sample effects on sW, we considered a normalized version of the distance by removing the expected sW over different sample sets from the true distribution.

better algorithm choice in SBI settings where the posterior score is unknown and has to be approximated. We include in Appendix F a complete analysis for the Gaussian example, comparing all algorithms for different choices of dimensions  $m$ , number of observations  $n$ , and precision  $\epsilon$ .

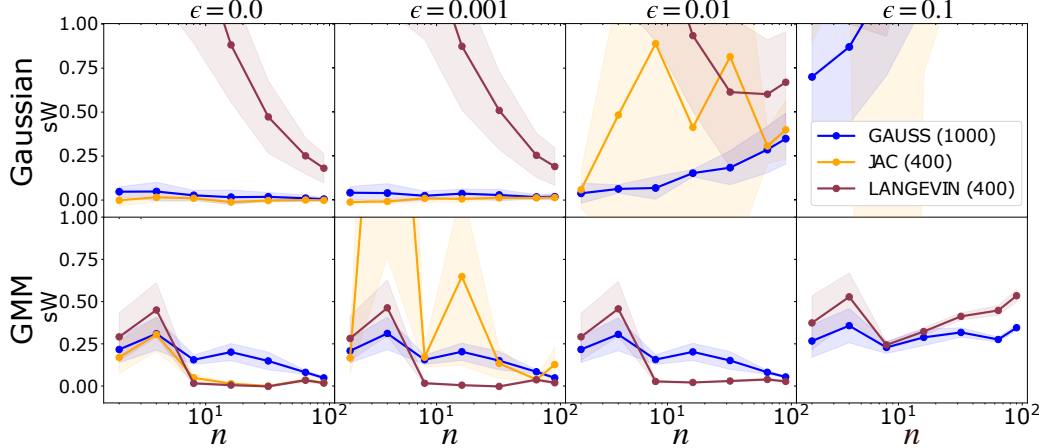


Figure 2: Normalized sW distance as a function of the number of observations  $n$  for the Gaussian and GMM toy examples, for each algorithm (**GAUSS**, **JAC** and **LANGEVIN**) and with different levels of  $\epsilon$ . Mean and std over 5 different seeds.

## 4.2 Benchmark SBI examples

We consider three examples from the increasingly popular SBI benchmark presented in Lueckmann et al. (2021b).

- SLCP ( $m = 5, d = 8$ ): Uniform prior and Gaussian simulator whose mean and covariance are non-linear functions of input parameter  $\theta$ .
- SIR ( $m = 2, d = 10$ ): LogNormal prior and simulator based on a set of differential equations and outputs sampled from a Binomial distribution.
- Lotka-Volterra ( $m = 4, d = 20$ ): LogNormal prior and simulator based on a set of differential equations and outputs sampled from a LogNormal output.

The score corresponding to each prior distribution is analytically computable; see Appendix D.<sup>6</sup> However, contrarily to the toy models from Section 4.1, the analytical posterior score is not available for the chosen examples and is, therefore, learned via score-matching (considering the loss function from Section 2.1).

Note that the purpose of the experiments in this section is not to find the best score model and the best posterior approximations for each task, which has already been done by Sharrock et al. (2022) and Geffner et al. (2023), but to evaluate the robustness of the different sampling algorithms. This is why we use the same score model architecture and training hyper parameters for all tasks, which may lead to different quality for the score estimator in each example (the data dimension and shape of the posterior impact the training of

<sup>6</sup>The LogNormal distribution can easily be transformed into a Gaussian distribution since when  $\theta \sim \text{LogNormal}(m, s)$  then  $\log \theta \sim \mathcal{N}(m, s)$ .

the score model). The used score model is always a MLP with 3 hidden layers, trained on  $N_{\text{train}}$  samples over 5000 epochs with Adam optimizer. We standardize the train data to have 0 mean and  $\mathbf{I}_m$  covariance matrix. This ensures that all the random variables  $\theta_t$  created during the generative process have 0 mean and  $\mathbf{I}_m$  covariance. Further details on the model architecture and training procedure are provided in Appendix E.

We use 1 000 sampling steps for **GAUSS** and **JAC**, and 400 steps for **LANGEVIN**. We also consider *clipped* versions for all proposed algorithms (represented with dotted lines in all figures), where the generated samples at each step are *clipped* between (-3,3) so to ensure that all samples stay within the region of high probability for the standard Gaussian distribution. We introduce this numerical procedure to stabilize the **JAC** and **LANGEVIN** algorithms, that we found to be less robust than **GAUSS**, with quickly diverging sW for poor score estimators; see Section 4.1. However, this procedure significantly slows down the sampling procedure and can introduce some bias in the posterior approximation.

Our empirical evaluation samples ten different ground truth parameters  $\theta^* \sim \lambda(\theta)$  from the prior distribution, each of which used to simulate observations  $x_j^* \sim p(x | \theta^*)$  for  $j = 1, \dots, n$ , later plugged in as conditioning variables in the tall posterior  $p(\theta | x_{1:n}^*)$ . For all three examples, samples from the true tall posterior can be obtained via MCMC using the `numpyro` package (Phan et al. (2019); Bingham et al. (2019)) and used to compute the sliced Wasserstein distance in every setting corresponding to varying  $N_{\text{train}}$  and  $n$ .

Figure 3 portrays the sW distance for each task as a function of the size  $N_{\text{train}}$  of the training set for the score model. Larger values of  $N_{\text{train}}$  are expected to yield better score estimates and thus more accurate posterior approximations. This is the case for `Lotka-Volterra`, where we observe a decreasing sW towards 0, for every  $n$ . For the two other examples, the rather constant behaviour indicates no learning (high sW values for `SLCP`) or an already close to optimal score model (low sW values for `SIR`).

**GAUSS** appears to be the most stable of the un-clipped methods and for poor score estimators (`SLCP` or `Lotka-Volterra` with small  $N_{\text{train}}$ ) **LANGEVIN** diverges as  $n$  increases. Note that **JAC** yields sW values that are always outside the plot limits. All clipped versions behave correctly. In Appendix G, Figure 8 shows the same results, but as a function the number of observations  $n \in [1, 8, 14, 22, 30]$  for a given score model (i.e. fixed  $N_{\text{train}}$ ). We also report results for the Maximum Mean Discrepancy (MMD) metric in Figures 9 and 10. Additionally, Figures 11 and 12 showcase the ability of the obtained posterior samples to concentrate (MMD to dirac) around the ground truth parameter  $\theta^*$ .

### 4.3 Inverting a non-linear model from computational neuroscience

We take one step further in the complexity of our numerical experiments and illustrate the Bayesian inversion of the Jansen & Rit neural mass model (JRNMM) Jansen and Rit (1995). Neural mass models are an important class of non-linear models from computational neuroscience that, based on physiologically motivated stochastic differential equations, are able to replicate oscillatory electrical signals experimentally observed with electroencephalography (EEG). These models are used as basic building blocks of large-scale simulators Sanz Leon et al. (2013) and are present in several simulation studies in cognitive and clinical neuroscience Aerts et al. (2018). We follow the setup proposed by Rodrigues et al. (2021). Specifically, we consider a stochastic version of the JRNMM Ableidinger et al. (2017) and use the C++ implementation in the supporting code of Buckwar et al. (2019). The output  $x(t)$  of this generative model is a time series obtained by taking as input a set of four parameters  $\theta = (C, \mu, \sigma, g)$ . Parameter  $C$  influences the general shape of the oscillatory behavior,  $(\mu, \sigma)$  dictate the amplitude and variance of the signals  $s(t)$  generated by the physiological model, and  $g$  represents a gain factor of an amplifier (resp. attenuator) used to measure the signals and produce the actual model output  $x(t) = 10^{g/10}s(t)$ . Here, the coupling-effect of parameters  $g$  and  $(\mu, \sigma)$  on the amplitude of the output signal  $x(t)$  leads to indeterminacy in the posterior inference

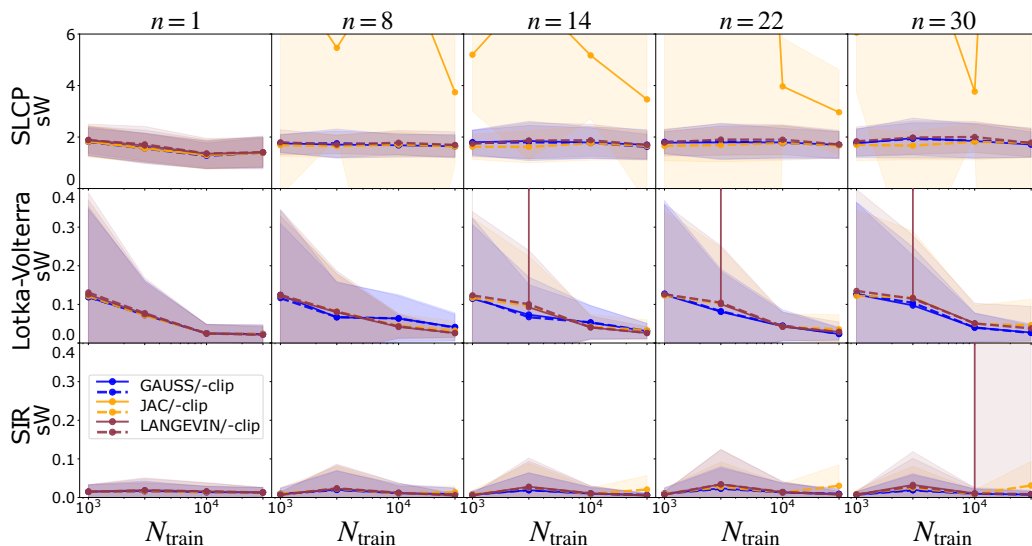


Figure 3: Curves with the sliced Wasserstein distance as a function of  $N_{\text{train}} \in [10^3, 3.10^3, 10^4, 3.10^4]$  between the samples obtained by each algorithm (**GAUSS**, **JAC** and **LANGEVIN**) and the true tall posterior distribution  $p(\theta \mid x_{1:n}^*)$  for  $n \in [1, 8, 14, 22, 30]$ . Mean and std over 10 different parameters  $\theta^* \sim \lambda(\theta)$ .

problem: the same observed signal  $x^*(t)$  could be generated with larger (smaller) values of  $g$  and smaller (larger) values of  $\mu$  and  $\sigma$ .

We now apply the different sampling algorithms **GAUSS**, **JAC** and **LANGEVIN** (and their clipped versions<sup>7</sup>), with respectively 1 000, 1 000 and 400 steps, to infer the posterior distribution of the JRNMM for a set of  $n$  observations  $x_j^* \sim p(x \mid \theta^*)$  independently simulated with  $\theta^* = (C^*, \mu^*, \sigma^*, g^*) = (125, 220, 2000, 0)$ . A uniform prior distribution is placed over the range of physiologically meaningful values of the simulator parameters as done in Buckwar et al. (2019); Rodrigues et al. (2021). The posterior score is again estimated using the model architecture and training procedure from Section 4.2. We evaluate the ability of our posterior approximator to concentrate around the true parameters  $\theta^*$ , which we quantify using the Maximum Mean Discrepancy (MMD) between the marginals of the approximate posterior and the Dirac distribution  $\delta_{\theta^*}$  centered at the true parameter  $\theta^*$ .

We first consider a simplified setting for which the gain parameter is fixed  $g = g^* = 0$  so to lift the indeterminacy on the estimation of parameters  $(\mu, \sigma)$ . Results are shown in Figure 4. On the left, we plot the MMD as a function of the number  $n$  of observations. **JAC** yields values outside of the plot limits. All other methods perform as wanted, with decreasing MMD. On the right are displayed the 1D marginals corresponding to the posterior samples obtained with **GAUSS** for observation sets  $x_{1:n}^*$  of increasing size. We observe a progressive concentration around  $\theta^*$ .

Figure 5 displays the results for the full 4-dimensional JRNMM. On the left plot, we can see that **GAUSS** yields consistently lower MMD values, with a decrease for lower  $n$ , **LANGEVIN** is unstable and **JAC** yields values outside of the plot limits. The 1D and 2D marginals for samples obtained for **GAUSS** are shown on the right. The non-decreasing behaviour of MMD for higher  $n$  can be explained by the indeterminacy in the inference task for the  $(\mu, \sigma)$  parameters, and is illustrated on the right plot, showing the 1D and 2D marginals

<sup>7</sup>Numerical procedure used to stabilize **JAC**; see Section 4.2.

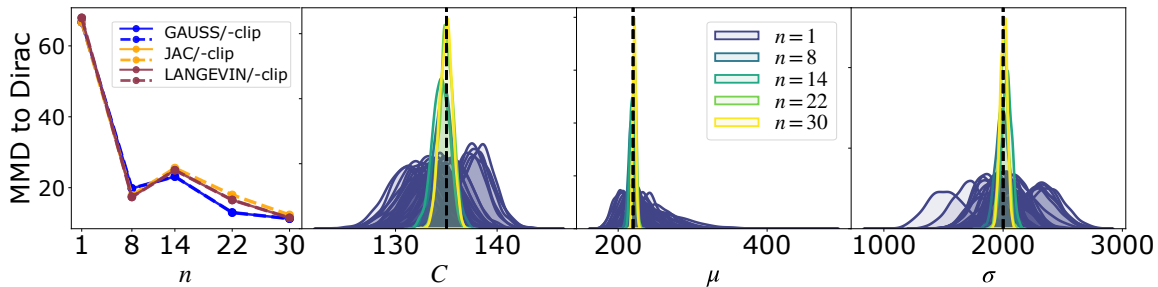


Figure 4: Inference on the 3D JRNMM (fixed  $g = 0$ ). Left: MMD between the marginals of the approximate posterior obtained for for **GAUSS**, **JAC**, and **LANGEVIN**, and the Dirac of the true parameters  $\theta^* = (125, 220, 2000)$  (black dotted lines) used to simulate the observations  $x_{1:n}^*$ . Right: Histograms of the 1D marginals of the posterior samples obtained with **GAUSS** for 30 single observations  $x_1^*, \dots, x_{30}^*$  ( $n = 1$ ) and for observation sets  $x_{1:n}^*$  of increasing size. We see that  $p(\theta | x_{1:n}^*)$  concentrates around  $\theta^*$ .

for samples obtained for **GAUSS**. Indeed, we observe a “sharpened banana” shaped posterior distribution, containing the true parameters, concentrated around  $C$  and  $g$ , but dispersed along the dimensions of  $(\mu, \sigma)$ .

## 5 Conclusion

In every experimental setting it is always desirable to leverage information from as much data as possible. Model inversions with SBI are no exception and the *tall data* extension considered in this paper provides a way of parsing extra observations in an efficient way. Indeed, our method only requires the training of an initial score model for a single observation to construct the score of the *tall data* posterior. This allows **GAUSS** and **JAC** to be more simulation efficient, avoiding the shortcomings of the augmented datasets required by **NPE**, **NLE**, and **NRE**. Moreover, we tackle directly the challenge of constructing a diffused version of the posterior distribution for *tall data* based on recently proposed second order approximations of the backward diffusion kernels. This is considerably different from what was proposed in Geffner et al. (2023), where the problem was simplified by constructing a sequence of distributions relying on the individual scores, but at the cost of drastically reducing the arsenal of samplers available for sampling from a Score based generative model. Indeed, our methodology can benefit from recent advances of score-diffusion literature, such as DDIM Song et al. (2021b), to perform backward sampling of the diffusion path and obtain samples from the posterior distribution in a much faster and stable way than the annealed Langevin procedure used in Geffner et al. (2023). We have illustrated the performance of our methods on different settings of increasing complexity, starting with toy examples for which the analytic posterior and scores were known, considering three examples from the SBI benchmark, and then finally applying the methodology to a challenging non-linear model from computational neuroscience. We demonstrated the superiority of our methods in terms of sample quality for almost all examples, and the reduced computational cost and increased numerical stability in every instance. Our work has confirmed the flexibility and viability of score-diffusion methods to approximate posterior distributions conditioned on sets of variable sizes and we expect that it will encourage other researchers to explore the score-diffusion framework for SBI problems.

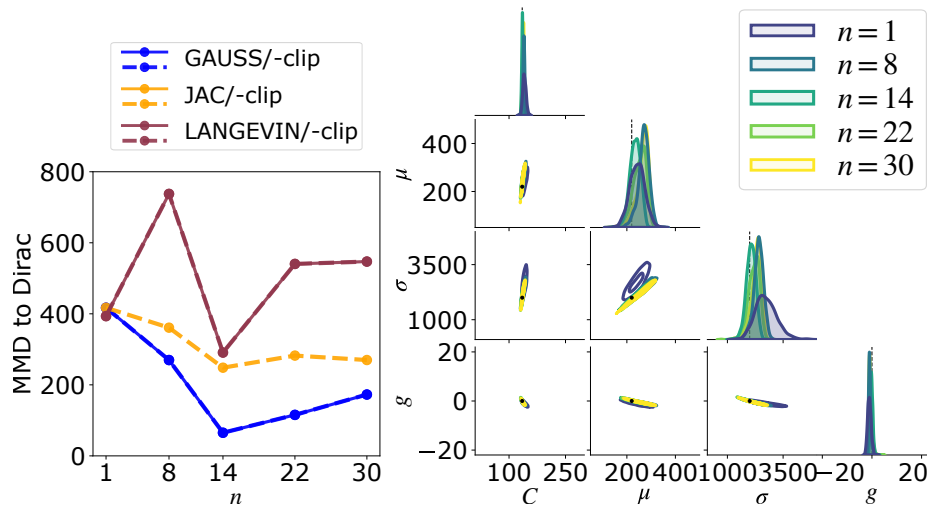


Figure 5: Inference on the full JRNMM. Left: MMD between the marginals of the approximate posterior obtained for **GAUSS**, **JAC**, and **LANGEVIN**, and the Dirac of the true parameters  $\theta^* = (125, 220, 2000, 0)$  used to simulate the observations  $x_{1:n}^*$ . Right: Histograms of the 1D and 2D marginals of the posterior samples obtained with **GAUSS** for a single observation  $x^*$  ( $n = 1$ ) and for sets  $x_{1:n}^*$  with increasing  $n$ . We observe a progressive convergence of the inferred posterior mean towards  $\theta^*$  (black dots), a sharpening around  $(C, g)$  and a sustained dispersion along the dimensions of  $(\mu, \sigma)$  due to JRNMM’s intrinsic indeterminacy.

## Acknowledgement

Numerical computation was enabled by the scientific Python ecosystem: NumPy (Harris et al., 2020), SciPy (Virtanen et al., 2020), Matplotlib (Hunter, 2007), Seaborn (Waskom, 2021), and PyTorch (Paszke et al., 2019). Julia Linhart is recipient of the Pierre-Aguilar Scholarship and thankful for the funding of the Capital Fund Management (CFM). The work of G.V. Cardoso is supported through the Investment of the Future grant, ANR-10-IAHU-04. Alexandre Gramfort thanks the support of the ANR BrAIN (ANR-20-CHIA0016) grant.

## References

- Ableidinger, M., Buckwar, E., and Hinterleitner, H. (2017). A stochastic version of the Jansen and Rit neural mass model: Analysis and numerics. *The Journal of Mathematical Neuroscience*, 7(1).
- Aerts, H., Schirner, M., Jeurissen, B., Van Roost, D., Achten, E., Ritter, P., and Marinazzo, D. (2018). Modeling brain dynamics in brain tumor patients using the virtual brain. *eNeuro*, 5(3). Society for Neuroscience.
- Bardenet, R., Doucet, A., and Holmes, C. (2015). On markov chain monte carlo methods for tall data. *Journal of Machine Learning Research*, 18:1–43.
- Batzolis, G., Stanczuk, J., and Schönlieb, C.-B. (2021). Conditional image generation with score-based diffusion models christian etmann deep render.

- Bhatia, R. (2006). *Positive definite matrices*. Princeton Series in Applied Mathematics. Princeton University Press, Princeton, NJ.
- Bingham, E., Chen, J. P., Jankowiak, M., Obermeyer, F., Pradhan, N., Karaletsos, T., Singh, R., Szerlip, P. A., Horsfall, P., and Goodman, N. D. (2019). Pyro: Deep universal probabilistic programming. *J. Mach. Learn. Res.*, 20:28:1–28:6.
- Boys, B., Girolami, M., Pidstrigach, J., Reich, S., Mosca, A., and Akyildiz, O. D. (2023). Tweedie moment projected diffusions for inverse problems. *arXiv preprint arXiv:2310.06721*.
- Buckwar, E., Tamborrino, M., and Tubikanec, I. (2019). Spectral density-based and measure-preserving ABC for partially observed diffusion processes. an illustration on hamiltonian SDEs. *Statistics and Computing*, 30(3):627–648.
- Cranmer, K., Brehmer, J., and Louppe, G. (2020). The frontier of simulation-based inference. *Proceedings of the National Academy of Sciences (PNAS)*, 117:30055–30062.
- Dax, M., Green, S. R., Gair, J., Pürerer, M., Wildberger, J., Macke, J. H., Buonanno, A., and Schölkopf, B. (2023). Neural importance sampling for rapid and reliable gravitational-wave inference. *Phys. Rev. Lett.*, 130:171403.
- Geffner, T., Papamakarios, G., and Mnih, A. (2023). Compositional score modeling for simulation-based inference.
- Gonçalves, P. J., Lueckmann, J.-M., Deistler, M., Nonnenmacher, M., Öcal, K., Bassetto, G., Chintaluri, C., Podlaski, W. F., Haddad, S. A., Vogels, T. P., Greenberg, D. S., and Macke, J. H. (2020). Training deep neural density estimators to identify mechanistic models of neural dynamics. *eLife*, 9:e56261.
- Goodfellow, I., Pouget-Abadie, J., Mirza, M., Xu, B., Warde-Farley, D., Ozair, S., Courville, A., and Bengio, Y. (2014). Generative adversarial nets. In Ghahramani, Z., Welling, M., Cortes, C., Lawrence, N., and Weinberger, K., editors, *Advances in Neural Information Processing Systems*, volume 27. Curran Associates, Inc.
- Greenberg, D., Nonnenmacher, M., and Macke, J. (2019). Automatic posterior transformation for likelihood-free inference. In Chaudhuri, K. and Salakhutdinov, R., editors, *Proceedings of the 36th International Conference on Machine Learning*, volume 97, pages 2404–2414. PMLR.
- Harris, C. R., Millman, K. J., van der Walt, S. J., Gommers, R., Virtanen, P., Cournapeau, D., Wieser, E., Taylor, J., Berg, S., Smith, N. J., Kern, R., Picus, M., Hoyer, S., van Kerkwijk, M. H., Brett, M., Haldane, A., del Río, J. F., Wiebe, M., Peterson, P., Gérard-Marchant, P., Sheppard, K., Reddy, T., Weckesser, W., Abbasi, H., Gohlke, C., and Oliphant, T. E. (2020). Array programming with NumPy. *585(7825):357–362*. Number: 7825 Publisher: Nature Publishing Group.
- Hermans, J., Begy, V., and Louppe, G. (2020). Likelihood-free MCMC with amortized approximate ratio estimators. In III, H. D. and Singh, A., editors, *Proceedings of the 37th International Conference on Machine Learning*, volume 119 of *Proceedings of Machine Learning Research*, pages 4239–4248. PMLR.
- Ho, J., Jain, A., and Abbeel, P. (2020). Denoising diffusion probabilistic models. *Advances in neural information processing systems*, 33:6840–6851.
- Ho, J. and Salimans, T. (2022). Classifier-free diffusion guidance.

- Hunter, J. D. (2007). Matplotlib: A 2d graphics environment. 9(3):90–95. Conference Name: Computing in Science & Engineering.
- Hyvärinen, A. and Dayan, P. (2005). Estimation of non-normalized statistical models by score matching. *Journal of Machine Learning Research*, 6(4).
- Jansen, B. H. and Rit, V. G. (1995). Electroencephalogram and visual evoked potential generation in a mathematical model of coupled cortical columns. *Biological Cybernetics 1995* 73:4, 73:357–366.
- Karras, T., Aittala, M., Aila, T., and Laine, S. (2022). Elucidating the design space of diffusion-based generative models. In *Proc. NeurIPS*.
- Lueckmann, J.-M., Boelts, J., Greenberg, D., Goncalves, P., and Macke, J. (2021a). Benchmarking simulation-based inference. In Banerjee, A. and Fukumizu, K., editors, *Proceedings of The 24th International Conference on Artificial Intelligence and Statistics*, volume 130 of *Proceedings of Machine Learning Research*, pages 343–351. PMLR.
- Lueckmann, J.-M., Boelts, J., Greenberg, D., Goncalves, P., and Macke, J. (2021b). Benchmarking simulation-based inference. In Banerjee, A. and Fukumizu, K., editors, *Proceedings of The 24th International Conference on Artificial Intelligence and Statistics*, volume 130 of *Proceedings of Machine Learning Research*, pages 343–351. PMLR.
- Papamakarios, G., Nalisnick, E., Rezende, D. J., Mohamed, S., and Lakshminarayanan, B. (2021). Normalizing flows for probabilistic modeling and inference. *Journal of Machine Learning Research*, 22:1–64.
- Papamakarios, G., Sterratt, D., and Murray, I. (2019). Sequential neural likelihood: Fast likelihood-free inference with autoregressive flows. 89:837–848.
- Paszke, A., Gross, S., Massa, F., Lerer, A., Bradbury, J., Chanan, G., Killeen, T., Lin, Z., Gimelshein, N., Antiga, L., Desmaison, A., Kopf, A., Yang, E., DeVito, Z., Raison, M., Tejani, A., Chilamkurthy, S., Steiner, B., Fang, L., Bai, J., and Chintala, S. (2019). PyTorch: An imperative style, high-performance deep learning library. In *Advances in Neural Information Processing Systems*, volume 32. Curran Associates, Inc.
- Phan, D., Pradhan, N., and Jankowiak, M. (2019). Composable effects for flexible and accelerated probabilistic programming in numpyro. *arXiv preprint arXiv:1912.11554*.
- Roberts, G. O. and Tweedie, R. L. (1996). Exponential convergence of langevin distributions and their discrete approximations. *Bernoulli*, pages 341–363.
- Rodrigues, P. L. C., Moreau, T., Louppe, G., and Gramfort, A. (2021). HNPE: Leveraging Global Parameters for Neural Posterior Estimation. In *NeurIPS 2021*, Sydney (Online), Australia.
- Sanz Leon, P., Knock, S., Woodman, M., Domide, L., Mersmann, J., McIntosh, A., and Jirsa, V. (2013). The virtual brain: a simulator of primate brain network dynamics. *Frontiers in Neuroinformatics*, 7:10.
- Sharrock, L., Simons, J., Liu, S., and Beaumont, M. (2022). Sequential neural score estimation: Likelihood-free inference with conditional score based diffusion models.
- Song, J., Meng, C., and Ermon, S. (2021a). Denoising diffusion implicit models. In *International Conference on Learning Representations*.



- Song, J., Vahdat, A., Mardani, M., and Kautz, J. (2023). Pseudoinverse-guided diffusion models for inverse problems. In *International Conference on Learning Representations*.
- Song, Y. and Ermon, S. (2019). Generative modeling by estimating gradients of the data distribution. *Advances in neural information processing systems*, 32.
- Song, Y., Sohl-Dickstein, J., Kingma, D. P., Kumar, A., Ermon, S., and Poole, B. (2020). Score-based generative modeling through stochastic differential equations. *ICLR 2021 - 9th International Conference on Learning Representations*.
- Song, Y., Sohl-Dickstein, J., Kingma, D. P., Kumar, A., Ermon, S., and Poole, B. (2021b). Score-based generative modeling through stochastic differential equations. In *International Conference on Learning Representations*.
- Tarantola, A. (2005). *Inverse Problem Theory and Methods for Model Parameter Estimation*. Society for Industrial and Applied Mathematics.
- Vasist, M., Rozet, F., Absil, O., Mollière, P., Nasedkin, E., and Louppe, G. (2023). Neural posterior estimation for exoplanetary atmospheric retrieval. *Astronomy and Astrophysics*, 672:A147.
- Vincent, P. (2011). A connection between score matching and denoising autoencoders. *Neural computation*, 23(7):1661–1674.
- Virtanen, P., Gommers, R., Oliphant, T. E., Haberland, M., Reddy, T., Cournapeau, D., Burovski, E., Peterson, P., Weckesser, W., Bright, J., van der Walt, S. J., Brett, M., Wilson, J., Millman, K. J., Mayorov, N., Nelson, A. R. J., Jones, E., Kern, R., Larson, E., Carey, C. J., Polat, I., Feng, Y., Moore, E. W., VanderPlas, J., Laxalde, D., Perktold, J., Cimrman, R., Henriksen, I., Quintero, E. A., Harris, C. R., Archibald, A. M., Ribeiro, A. H., Pedregosa, F., and van Mulbregt, P. (2020). SciPy 1.0: fundamental algorithms for scientific computing in python. 17(3):261–272. Number: 3 Publisher: Nature Publishing Group.
- Waskom, M. L. (2021). seaborn: statistical data visualization. 6(60):3021.
- Yang, L., Zhang, Z., Song, Y., Hong, S., Xu, R., Zhao, Y., Zhang, W., Cui, B., and Yang, M.-H. (2023). Diffusion models: A comprehensive survey of methods and applications. *ACM Computing Surveys*, 56(4):1–39.
- Zaheer, M., Kottur, S., Ravanbakhsh, S., Póczos, B., Salakhutdinov, R. R., and Smola, A. J. (2017). Deep sets. In Guyon, I., Luxburg, U. V., Bengio, S., Wallach, H., Fergus, R., Vishwanathan, S., and Garnett, R., editors, *Advances in Neural Information Processing Systems*, volume 30. Curran Associates, Inc.

## A Proofs

### A.1 Proof of Lemma 3.1

Let  $(\mu_k)_{1 \leq k \leq K} \in (\mathbb{R}^m)^K$  and  $(\Sigma_k)_{1 \leq k \leq K}$  be covariance matrices in  $\mathbb{R}^{m \times m}$ . Denote by  $p_k$  the Gaussian pdf with mean  $\mu_k$  and covariance matrix  $\Sigma_k$ . Note that

$$p_k : \theta_0 \mapsto \exp \left( \tilde{\zeta}_k + (\Sigma_k^{-1} \mu_k)^\top \theta_0 - \frac{1}{2} \theta_0^\top \Sigma_k^{-1} \theta_0 \right),$$

where

$$\tilde{\zeta}_k = -\frac{1}{2} (m \log 2\pi - \log |\Sigma_k^{-1}| + \mu_k^\top \Sigma_k^{-1} \mu_k).$$

Therefore,

$$\begin{aligned} \prod_{k=1}^K p_k(\theta_0) &= \exp \left( \sum_{k=1}^K \tilde{\zeta}_k - \tilde{\zeta}_{\text{all}} \right) \exp \left( \tilde{\zeta}_{\text{all}} + \tilde{\eta}^\top \theta_0 - \frac{1}{2} \theta_0^\top \tilde{\Lambda} \theta_0 \right) \\ &= \exp \left( \sum_{k=1}^K \tilde{\zeta}_k - \tilde{\zeta}_{\text{all}} \right) \mathcal{N}(\theta_0; \tilde{\Lambda}^{-1} \tilde{\eta}, \tilde{\Lambda}^{-1}), \end{aligned}$$

with  $\tilde{\eta} = \sum_{k=1}^K \Sigma_k^{-1} \mu_k$ ,  $\tilde{\Lambda} = \sum_{k=1}^K \Sigma_k^{-1}$ , and  $\tilde{\zeta}_{\text{all}} = -(m \log 2\pi - \log |\tilde{\Lambda}| + \tilde{\eta}^\top \tilde{\Lambda}^{-1} \tilde{\eta})/2$ . We can apply this result to equation (12) with

$$\begin{aligned} \eta(\theta) &= \sum_{j=1}^n \Sigma_t^{-1}(\theta, x_j) \mu_t(\theta, x_j) + (1-n) \Sigma_{t,\lambda}^{-1}(\theta) \mu_{t,\lambda}(\theta), \\ \Lambda(\theta) &= \sum_{j=1}^n \Sigma_t^{-1}(\theta, x_j) + (1-n) \Sigma_{t,\lambda}^{-1}(\theta), \end{aligned}$$

since by assumption  $\Lambda(\theta)$  is definite positive. This provides the following reformulation of equation (12):

$$\ell_\lambda(\theta, x_{1:n}^*) = \log \int \exp \left( \sum_{j=1}^n \zeta_j(\theta) + (1-n) \zeta_\lambda(\theta) - \zeta_{\text{all}}(\theta) \right) \mathcal{N}(\theta_0; \Lambda^{-1}(\theta) \eta(\theta), \Lambda^{-1}(\theta)) d\theta_0,$$

which concludes the proof.

### A.2 Proof of Lemma 3.2

Let  $\zeta(\mu, \Sigma^{-1}) = -(m \log 2\pi - \log |\Sigma^{-1}| + \mu^\top \Sigma^{-1} \mu) / 2$ . Then,

$$\begin{aligned} \nabla_\theta \zeta_j(\theta, x_j) &= \nabla_\theta \zeta(\mu_t(\theta, x_j), \Sigma_t^{-1}(\theta, x_j)) \\ &= \nabla_\mu \zeta(\mu_t(\theta, x_j), \Sigma_t^{-1}(\theta, x_j))^\top \nabla_\theta \mu_t(\theta, x_j) \\ &\quad + \nabla_{\Sigma^{-1}} \zeta(\mu_t(\theta, x_j), \Sigma_t^{-1}(\theta, x_j)) \nabla_\theta \Sigma_t^{-1}(\theta, x_j), \end{aligned}$$

where

$$\begin{aligned}\nabla_{\mu}\zeta(\mu, \Sigma^{-1}) &= -\Sigma^{-1}\mu \\ \nabla_{\Sigma}^{-1}\zeta(\mu, \Sigma^{-1}) &= (1/2) (\Sigma - \mu\mu^{\top}).\end{aligned}$$

Therefore, we obtain

$$\begin{aligned}\nabla_{\theta}\zeta_j(\theta, x_j) &= -\mu_t(\theta, x_j)^{\top}\Sigma_t^{-1}(\theta, x_j)^{\top}\nabla_{\theta}\mu_t(\theta, x_j) \\ &\quad + (1/2) (\Sigma_t(\theta, x_j) - \mu_t(\theta, x_j)\mu_t(\theta, x_j)^{\top}) \nabla_{\theta}\Sigma_t^{-1}(\theta, x_j).\end{aligned}$$

Note that  $\nabla_{\theta}\mu_t(\theta, x_j) = (\sqrt{\alpha_t}/v_t)\Sigma_t(\theta, x_j)$ , which leads to

$$\begin{aligned}\nabla_{\theta}\zeta_j(\theta, x_j) &= -\frac{\sqrt{\alpha_t}}{v_t}\mu_t(\theta, x_j) + (1/2) (\Sigma_t(\theta, x_j) - \mu_t(\theta, x_j)\mu_t(\theta, x_j)^{\top}) \nabla_{\theta}\Sigma_t^{-1}(\theta, x_j) \\ &= -v_t^{-1}\theta - \nabla_{\theta}\log p_t(\theta)x_j + (1/2) (\Sigma_t(\theta, x_j) - \mu_t(\theta, x_j)\mu_t(\theta, x_j)^{\top}) \nabla_{\theta}\Sigma_t^{-1}(\theta, x_j).\end{aligned}$$

This leads to

$$\begin{aligned}\nabla_{\theta}\ell_{\lambda}(\theta, x_{1:n}) &= -(1-n)\nabla_{\theta}\log p_t^{\lambda}(\theta) - \sum_{j=1}^n \nabla_{\theta}\log p_t(\theta)x_j^* - v_t^{-1}\theta - \nabla_{\theta}\zeta_{\text{all}}(\theta) \\ &\quad + (1/2) \left[ \sum_{j=1}^n (\Sigma_t(\theta, x_j) - \mu_t(\theta, x_j)\mu_t(\theta, x_j)^{\top}) \nabla_{\theta}\Sigma_t^{-1}(\theta, x_j) \right] \\ &\quad + \frac{1-n}{2} (\Sigma_{t,\lambda}(\theta) - \mu_{t,\lambda}(\theta)\mu_{t,\lambda}(\theta)^{\top}) \nabla_{\theta}\Sigma_{t,\lambda}^{-1}(\theta, x_j).\end{aligned}$$

The score is then given by

$$\begin{aligned}\nabla_{\theta}\log p_t(\theta)x_{1:n} &= -v_t^{-1}\theta - \nabla_{\theta}\zeta_{\text{all}}(\theta) \\ &\quad + (1/2) \left[ \sum_{j=1}^n (\Sigma_t(\theta, x_j) - \mu_t(\theta, x_j)\mu_t(\theta, x_j)^{\top}) \nabla_{\theta}\Sigma_t^{-1}(\theta, x_j) \right] \\ &\quad + \frac{1-n}{2} (\Sigma_{t,\lambda}(\theta) - \mu_{t,\lambda}(\theta)\mu_{t,\lambda}(\theta)^{\top}) \nabla_{\theta}\Sigma_{t,\lambda}^{-1}(\theta, x_j).\end{aligned}$$

We now estimate  $\nabla_{\theta}\zeta_{\text{all}}(\theta)$  by noting that  $\zeta_{\text{all}} = \zeta(\Lambda(\theta)^{-1}\eta(\theta), \Lambda(\theta))$ . We obtain

$$\begin{aligned}\nabla_{\theta}\zeta_{\text{all}}(\theta) &= -\nabla_{\theta}(\Lambda(\theta)^{-1}\eta(\theta))\eta(\theta) + (1/2) [\text{Id} - \Lambda(\theta)^{-1}\eta(\theta)\eta(\theta)^{\top}] \Lambda(\theta)^{-1}\nabla_{\theta}\Lambda(\theta) \\ &= -\Lambda(\theta)^{-1}\nabla_{\theta}\eta(\theta)\eta(\theta) - \eta(\theta)^{\top}\nabla\Lambda(\theta)^{-1}\eta(\theta) + (1/2) [\text{Id} - \Lambda(\theta)^{-1}\eta(\theta)\eta(\theta)^{\top}] \Lambda(\theta)^{-1}\nabla_{\theta}\Lambda(\theta).\end{aligned}$$

Note now that

$$\begin{aligned}\nabla_{\theta}\eta(\theta) &= \sum_{j=1}^n \Sigma_t^{-1}(\theta, x_j)\nabla_{\theta}\mu_t(\theta, x_j) + \mu_t(\theta, x_j)^{\top}\nabla_{\theta}\Sigma_t^{-1}(\theta, x_j) \\ &\quad + (1-n) \left( \Sigma_{t,\lambda}^{-1}(\theta)\nabla_{\theta}\mu_{t,\lambda}(\theta) + \mu_{t,\lambda}(\theta)^{\top}\nabla_{\theta}\Sigma_{t,\lambda}^{-1}(\theta) \right) \\ &= \frac{\sqrt{\alpha_t}}{v_t}\text{Id} + \sum_{j=1}^n \mu_t(\theta, x_j)^{\top}\nabla_{\theta}\Sigma_t^{-1}(\theta, x_j) + (1-n)\mu_{t,\lambda}(\theta)^{\top}\nabla_{\theta}\Sigma_{t,\lambda}^{-1}(\theta),\end{aligned}$$

which leads to

$$\nabla_{\theta} \eta(\theta) \eta(\theta) = \frac{\sqrt{\alpha_t}}{v_t} \eta(\theta) + \left[ \sum_{j=1}^n \mu_t(\theta, x_j)^{\top} \nabla_{\theta} \Sigma_t^{-1}(\theta, x_j) + (1-n) \mu_{t,\lambda}(\theta)^{\top} \nabla_{\theta} \Sigma_{t,\lambda}^{-1}(\theta) \right] \eta(\theta). \quad (14)$$

Note that

$$\begin{aligned} \sqrt{\alpha_t} \eta(\theta) &= \sum_{j=1}^n \Sigma_t^{-1}(\theta, x_j) (\theta + v_t \nabla_{\theta} \log p_t(\theta) x_j) + (1-n) \Sigma_{t,\lambda}^{-1}(\theta) (\theta + v_t \nabla_{\theta} \log p_t^{\lambda}(\theta)) \\ &= \Lambda(\theta) \theta + v_t \left[ \sum_{j=1}^n \Sigma_t^{-1}(\theta, x_j) \nabla_{\theta} \log p_t(\theta) x_j + (1-n) \Sigma_{t,\lambda}^{-1}(\theta) \nabla_{\theta} \log p_t^{\lambda}(\theta) \right], \end{aligned}$$

which finally leads to

$$\nabla_{\theta} \log p_t(\theta | x_{1:n}^*) = \Lambda(\theta)^{-1} \left[ \sum_{j=1}^n \Sigma_t^{-1}(\theta, x_j) \nabla_{\theta} \log p_t(\theta) x_j + (1-n) \Sigma_{t,\lambda}^{-1}(\theta) \nabla_{\theta} \log p_t^{\lambda}(\theta) \right] + F(\theta, x_{1:n}^*),$$

where

$$\begin{aligned} F(\theta, x_{1:n}^*) &= \eta(\theta)^{\top} \nabla \Lambda(\theta)^{-1} \eta(\theta) + (1/2) [\text{Id} - \Lambda(\theta)^{-1} \eta(\theta) \eta(\theta)^{\top}] \Lambda(\theta)^{-1} \nabla_{\theta} \Lambda(\theta) \\ &\quad + (1/2) \left[ \sum_{j=1}^n (\Sigma_t(\theta, x_j) - \mu_t(\theta, x_j) \mu_t(\theta, x_j)^{\top}) \nabla_{\theta} \Sigma_t^{-1}(\theta, x_j) \right] \\ &\quad + \frac{1-n}{2} (\Sigma_{t,\lambda}(\theta) - \mu_{t,\lambda}(\theta) \mu_{t,\lambda}(\theta)^{\top}) \nabla_{\theta} \Sigma_{t,\lambda}^{-1}(\theta, x_j). \end{aligned}$$

## B Positive Definiteness of $\Lambda(\theta)$

The approximation described in Section 3.2 is only valid if matrix  $\Lambda(\theta)$  is symmetric positive definite (SPD), i.e. it is a valid covariance matrix. In what follows, we will show what are the conditions on the choice of the pdf for the prior distribution that will ensure such property. Using the partial ordering defined by the convex cone of SPD matrices Bhatia (2006) it follows that:

$$\Lambda(\theta) \succ 0 \iff \sum_{j=1}^n \Sigma_t^{-1}(\theta, x_j) + (1-n) \Sigma_{t,\lambda}^{-1}(\theta) \succ 0, \quad (15)$$

$$\iff \sum_{j=1}^n \Sigma_t^{-1}(\theta, x_j) \succ (n-1) \Sigma_{t,\lambda}^{-1}(\theta), \quad (16)$$

$$\iff \Sigma_{t,\lambda}(\theta) \succ \left( \frac{1}{(n-1)} \sum_{j=1}^n \Sigma_t^{-1}(\theta, x_j) \right)^{-1}. \quad (17)$$

Note that as  $n$  increases, the R.H.S. of the inequality converges to the harmonic mean of the  $\Sigma_t(\theta, x_j)$ , which helps building an intuition to the correct choice for the covariance  $\Sigma_{t,\lambda}(\theta)$  of the prior. For instance,

a sufficient choice (not necessarily optimal) would be to have a  $\Sigma_{t,\lambda}(\theta)$  whose associated ellipsoid<sup>8</sup> covers the ellipsoids generated by all other covariance matrices  $\Sigma_t(\theta, x_j)$ .

## C Influence of the correction term $\nabla_{\theta} \ell_{\lambda}(\theta, x_{1:n}^*)$ .

Intuition following the definition of the backward kernels in equation (8):

- For  $t \rightarrow 1$ : the forward kernel and the diffused data distribution get close to the noise distribution:  $p_t(\theta | x) \xrightarrow{t \rightarrow 1} \mathcal{N}(\theta; 0, \mathbf{I}_m)$  and  $q_{t|0}(\theta | \theta_0) \xrightarrow{t \rightarrow 1} \mathcal{N}(\theta; 0, \mathbf{I}_m)$ . Therefore the backward kernel is approximately the target data distribution:

$$p_{0|t}(\theta_0 | \theta, x) = \frac{p(\theta_0 | x) q_{t|0}(\theta | \theta_0)}{p_t(\theta | x)} \underset{t \rightarrow 1}{\sim} p(\theta_0 | x). \quad (18)$$

Therefore the backward kernels vary very little with  $\theta$ , and because they define  $\ell_{\lambda}(\theta, x_{1:n}^*)$  (see eq. (12)), its gradient is close to zero. In other words,  $\nabla_{\theta} \ell_{\lambda}(\theta, x_{1:n}^*)$  has no significant impact at the beginning of the backward diffusion (aka. sampling or generative process).

- For  $t \rightarrow 0$ : the denominator is the diffused distribution that gets close to the target data distribution  $p_t(\theta | x) \xrightarrow{t \rightarrow 0} p(\theta_0 | x)$ . Therefore the backward kernel is approximately

$$p_{0|t}(\theta_0 | \theta, x) = \frac{p(\theta_0 | x) q_{t|0}(\theta | \theta_0)}{p_t(\theta | x)} \underset{t \rightarrow 0}{\sim} q_{t|0}(\theta | \theta_0) \xrightarrow{t \rightarrow 0} \delta_{\theta_0}(\theta). \quad (19)$$

Here, the dependence on  $\theta$  is convergence to a dirac function. Which means that the gradient of  $\ell_{\lambda}(\theta, x_{1:n}^*)$  will increase during the sampling process and finally explode when  $t$  approaches 0. The correction term therefore plays an important role as we approach the target tall data posterior distribution, at the end of the sampling process.

## D Analytical formulas for score and related quantities

### D.1 Gaussian case

The considered Bayesian Inference task is to estimate the mean  $\theta \in \mathbb{R}^m$  of a Gaussian simulator model  $p(x | \theta) = \mathcal{N}(x; \theta, \Sigma)$ , given a Gaussian prior  $\lambda(\theta) = \mathcal{N}(\theta; \mu_{\lambda}, \Sigma_{\lambda})$ . For a single observation  $x^*$ , the true posterior is also a Gaussian obtained using Bayes formula, as the product of two Gaussian distributions:

$$p(\theta | x^*) = \mathcal{N}(\theta; \mu_{\text{post}}(x^*), \Sigma_{\text{post}}) \quad (20)$$

with  $\mu_{\text{post}}(x^*) = \Sigma_{\text{post}}(\Sigma^{-1}x^* + \Sigma_{\lambda}^{-1}\mu_{\lambda})$  and  $\Sigma_{\text{post}} = (\Sigma^{-1} + \Sigma_{\lambda}^{-1})^{-1}$ . Note that in this case, the full posterior can be written as

$$p(\theta | x_{1:n}^*) = \mathcal{N}(\theta; \mu_{\text{post}}(x_{1:n}^*), \Sigma_{\text{post},n}) \quad (21)$$

with  $\Sigma_{\text{post},n} = (n\Sigma^{-1} + \Sigma_{\lambda}^{-1})^{-1}$  and  $\mu_{\text{post}}(x_{1:n}^*) = \Sigma_{\text{post},n}(\sum_{j=1}^n \Sigma^{-1}x_j^* + \Sigma_{\lambda}^{-1}\mu_{\lambda})$ .

<sup>8</sup>The ellipsoid  $\mathcal{E}_A$  associated with SPD matrix  $A$  is defined as  $\mathcal{E}_A = \{\mathbf{x} : \mathbf{x}^{\top} A^{-1} \mathbf{x} < 1\}$

Assume that  $q_{t|0}(\theta | \theta_0) = \mathcal{N}(\theta; \sqrt{\alpha_t}\theta_0, v_t\mathbf{I}_m)$ ; see Section 2. Using standard results (e.g. equation 2.115 in Bishop, 2006), we can derive the analytic formula of the diffused prior

$$p_t^\lambda(\theta) = \int \lambda(\theta_0)q_{t|0}(\theta | \theta_0)d\theta_0 \quad (22)$$

$$= \mathcal{N}(\theta; \sqrt{\alpha_t}\mu_\lambda, \alpha_t\Sigma_\lambda + v_t\mathbf{I}_m) \quad (23)$$

and of the diffused posterior

$$p_t(\theta | x^*) = \int p(\theta_0 | x^*)q_{t|0}(\theta | \theta_0)d\theta_0 \quad (24)$$

$$= \mathcal{N}(\theta; \sqrt{\alpha_t}\mu_{\text{post}}(x^*), \alpha_t\Sigma_{\text{post}} + v_t\mathbf{I}_m). \quad (25)$$

The corresponding Fisher scores are

$$\nabla_\theta \log p_t^\lambda(\theta) = -(\alpha_t\Sigma_\lambda + v_t\mathbf{I}_m)^{-1}(\theta - \sqrt{\alpha_t}\mu_\lambda), \quad (26)$$

$$\nabla_\theta \log p_t(\theta | x^*) = -(\alpha_t\Sigma_{\text{post}} + v_t\mathbf{I}_m)^{-1}(\theta - \sqrt{\alpha_t}\mu_{\text{post}}(x^*)). \quad (27)$$

Replacing the score from (27) in the formulas from Boys et al. (2023), we get the following expressions for the mean and covariance matrix of the posterior backward diffusion kernel  $p_{0|t}(\theta_0 | \theta, x)$ :

$$\begin{aligned} \Sigma_t(\theta, x^*) &= \frac{v_t}{\alpha_t} \left( 1 - v_t \left( \alpha_t \Sigma_{\text{post}} + v_t \mathbf{I}_m \right)^{-1} \right) = \Sigma_t, \\ \mu_t(\theta, x^*) &= \frac{1}{\sqrt{\alpha_t}} \left( 1 - v_t \left( \alpha_t \Sigma_{\text{post}} + v_t \mathbf{I}_m \right)^{-1} \right) \theta + v_t \left( \alpha_t \Sigma_{\text{post}} + v_t \mathbf{I}_m \right)^{-1} \mu_{\text{post}}(x^*) \\ &= \frac{\sqrt{\alpha_t}}{v_t} \Sigma_t \theta + v_t \left( \alpha_t \Sigma_{\text{post}} + v_t \mathbf{I}_m \right)^{-1} \mu_{\text{post}}(x^*). \end{aligned}$$

The same goes for the prior backward diffusion kernel  $p_{0|t}^\lambda(\theta_0 | \theta)$ :

$$\begin{aligned} \Sigma_{t,\lambda}(\theta) &= \frac{v_t}{\alpha_t} \left( 1 - v_t \left( \alpha_t \Sigma_\lambda + v_t \mathbf{I}_m \right)^{-1} \right) = \Sigma_{t,\lambda}, \\ \mu_{t,\lambda}(\theta) &= \frac{1}{\sqrt{\alpha_t}} \left( 1 - v_t \left( \alpha_t \Sigma_\lambda + v_t \mathbf{I}_m \right)^{-1} \right) \theta + v_t \left( \alpha_t \Sigma_\lambda + v_t \mathbf{I}_m \right)^{-1} \mu_\lambda \\ &= \frac{\sqrt{\alpha_t}}{v_t} \Sigma_{t,\lambda} \theta + v_t \left( \alpha_t \Sigma_\lambda + v_t \mathbf{I}_m \right)^{-1} \mu_\lambda. \end{aligned}$$

We now consider the tall data setting with  $n$  i.i.d. observations  $x_{1:n}^* = \{x_1^*, \dots, x_n^*\}$  and compute the correction term  $\nabla_\theta \ell_\lambda(\theta, x_{1:n}^*)$ . Note that the covariance matrices above are independent of  $\theta$  and therefore  $\Lambda(\theta)$  does not depend on  $\theta$  and is referred to as  $\Lambda$ . Consequently, we only need to consider the terms that depend on the means  $\mu_t(\theta, x_j^*)$  or  $\mu_{t,\lambda}(\theta)$  when computing the gradient w.r.t.  $\theta$ .

$$\nabla \zeta_{0|t}(\theta, x) = -\frac{\sqrt{\alpha_t}}{v_t} \mu_t(\theta, x), \quad (28)$$

$$\nabla \zeta_{0|t,\lambda}(\theta) = -\frac{\sqrt{\alpha_t}}{v_t} \mu_{t,\lambda}(\theta). \quad (29)$$

For  $\zeta_{0|t,\text{all}}$ , write

$$\begin{aligned}
\eta_{0|t}(\theta) &= \sum_{j=1}^N \Sigma_t^{-1} \left[ \frac{\sqrt{\alpha_t}}{v_t} \Sigma_t \theta + v_t \left( \alpha_t \Sigma_{\text{post}} + v_t \mathbf{I}_m \right)^{-1} \mu_{\text{post}}(x_j^*) \right] \\
&\quad + (1-n) \Sigma_{t,\lambda}^{-1} \left[ \frac{\sqrt{\alpha_t}}{v_t} \Sigma_{t,\lambda} \theta + v_t \left( \alpha_t \Sigma_\lambda + v_t \mathbf{I}_m \right)^{-1} \mu_\lambda \right] \\
&= \frac{\sqrt{\alpha_t}}{v_t} \theta + v_t \Sigma_t^{-1} \left( \alpha_t \Sigma_{\text{post}} + v_t \mathbf{I}_m \right)^{-1} \sum_{j=1}^N \mu_{\text{post}}(x_j^*) \\
&\quad + (1-n) v_t \Sigma_{t,\lambda}^{-1} \left( \alpha_t \Sigma_\lambda + v_t \mathbf{I}_m \right)^{-1} \mu_\lambda.
\end{aligned}$$

We need to assure the positive definiteness of  $\Lambda(\theta)$ . Let  $v \in \mathbb{R}^d$  such that  $\|v\| = 1$ . Thus,

$$v^\top \Lambda(\theta) v \propto \frac{1}{v_t} + \alpha_t^2 (1-n) v^\top \Sigma_\lambda v + n \alpha_t^2 v^\top \Sigma_{\text{post}} v. \quad (30)$$

Therefore, for  $\Lambda(\theta)$  to be positive definite is equivalent to

$$v^\top \Sigma_{\text{post}} v > \frac{n-1}{n} v^\top \Sigma_\lambda v - \frac{1}{n v_t \alpha_t^2}, \quad (31)$$

for all  $v \in \mathbb{R}^d$  such that  $\|v\| = 1$ . Note that it is not trivial to find meaningful worst case scenario sufficient condition for the inequality above. To see why, let  $e_{\text{post}}^{\min}$  be the smallest eigenvalue of  $\Sigma_{\text{post}}$  and  $e_\lambda^{\max}$  the biggest eigenvalue of  $\Sigma_\lambda$ . Then, a sufficient condition would be  $e_\lambda^{\max} < e_{\text{post}}^{\min}$ , since

$$v^\top \Sigma_{\text{post}} v > e_{\text{post}}^{\min} > e_\lambda^{\max} > \frac{n-1}{n} v^\top \Sigma_\lambda v - \frac{1}{n v_t \alpha_t^2}. \quad (32)$$

But this does not makes much sense, since we are asking the prior to be more concentrated than the posterior! Therefore, we obtain  $\nabla \zeta_{0|t,\text{all}} = -\sqrt{\alpha_t} \Lambda^{-1} \eta_{0|t}(\theta) / v_t$ , which yields

$$\nabla \ell_\lambda(\theta, x_{1:n}^*) = -\frac{\sqrt{\alpha_t}}{v_t} \left( \sum_{j=1}^n \mu_t(\theta, x_j^*) + (1-n) \mu_{t,\lambda}(\theta) - \Lambda^{-1} \eta_{0|t}(\theta) \right). \quad (33)$$

## D.2 Score of the diffused Uniform prior

Consider the case where the prior is a Uniform distribution  $\lambda(\theta) = \mathcal{U}(\theta; a, b)$ , with  $(a, b) \in \mathbb{R}^m \times \mathbb{R}^m$ , the lower and upper bounds respectively. Assume that  $q_{t|0}(\theta | \theta_0) = \mathcal{N}(\theta; \sqrt{\alpha_t} \theta_0, v_t \mathbf{I}_m)$ ; see Section 2 with  $v_t = 1 - \alpha_t$ . We then get the following analytic formula for the diffused prior:

$$p_t^\lambda(\theta) = \int \lambda(\theta_0) q_{t|0}(\theta | \theta_0) d\theta_0 \quad (34)$$

$$= \frac{1}{\prod_{i=1}^m (b_i - a_i)} \int_{[a_1, b_1] \times \dots \times [a_m, b_m]} \mathcal{N}(\theta; \sqrt{\alpha_t} \theta_0, v_t \mathbf{I}_m) \quad (35)$$

$$= \frac{1}{\sqrt{\alpha_t} \prod_{i=1}^m (b_i - a_i)} \prod_{i=1}^m (\Phi(\sqrt{\alpha_t} b_i; \theta_i, v_t) - \Phi(\sqrt{\alpha_t} a_i; \theta_i, v_t)), \quad (36)$$

where  $\Phi(\cdot; \mu, \sigma^2)$  is the c.d.f. of a univariate Gaussian with mean  $\mu$  and variance  $\sigma^2$ . The score of the above quantity is then simply obtained by computing the score of each one-dimensional element in the above product. For  $i \in [1, m]$ ,  $\nabla_{\theta} \log p_t^{\lambda}(\theta)_i = \nabla_{\theta_i} \log f(\theta_i) = \frac{\nabla_{\theta_i} f(\theta_i)}{f(\theta_i)}$  with

$$f(\theta_i) = (\Phi(\sqrt{\alpha_t} b_i; \theta_i, v_t) - \Phi(\sqrt{\alpha_t} a_i; \theta_i, v_t)) \quad (37)$$

$$\nabla_{\theta_i} f(\theta_i) = -\frac{1}{\sqrt{\alpha_t v_t}} (\mathcal{N}(\sqrt{\alpha_t} b_i; \theta_i, v_t) - \mathcal{N}(\sqrt{\alpha_t} a_i; \theta_i, v_t)). \quad (38)$$

### D.3 Mixture of Gaussians

In the case of the Mixture of Gaussians, the prior is  $\lambda = \mathcal{N}(0, \text{Id})$ , the simulator is given by  $p(x|\theta) = (1/2)\mathcal{N}(x; \theta, \Sigma_1) + (1/2)\mathcal{N}(x; \theta, 1/9\Sigma_2)$  where  $\Sigma_1 = 2.25\Sigma$ ,  $\Sigma_2 = 1/9\Sigma$  and  $\Sigma$  is a diagonal matrix with values increasing linearly between 0.6 and 1.4. In this case, the posterior pdf is

$$p(\theta|x) = \omega_1(x)\mathcal{N}(\theta; \mu_1, \Sigma_{1,p}) + \omega_2(x)\mathcal{N}(\theta; \mu_2, \Sigma_{2,p}) \quad (39)$$

where for  $i = 1, 2$ ,  $\Sigma_{i,p} = (\Sigma_i^{-1} + \text{Id})^{-1}$ ,  $\mu_i = \Sigma_{i,p}\Sigma_i^{-1}x$ ,  $\tilde{\omega}_i(x) = \mathcal{N}(x; \theta, \Sigma_i + \text{Id})$  and  $\omega_i = \tilde{\omega}_i / \sum_{j=1}^2 \tilde{\omega}_j$ .

Therefore, the diffused marginals are

$$p_t(\theta|x) = \omega_1(x)\mathcal{N}(\theta; \alpha_t^{1/2}\mu_1, \alpha_t\Sigma_{1,p} + (1 - \alpha_t)\text{Id}) + \omega_2(x)\mathcal{N}(\theta; \alpha_t^{1/2}\mu_2, \alpha_t\Sigma_{2,p} + (1 - \alpha_t)\text{Id}), \quad (40)$$

from which the score is

$$\nabla_{\theta} \log p_t(\theta|x) = -\omega_1(x)(\alpha_t\Sigma_{1,p} + (1 - \alpha_t)\text{Id})^{-1}(\theta - \alpha_t^{1/2}\mu_1) - \omega_2(x)(\alpha_t\Sigma_{2,p} + (1 - \alpha_t)\text{Id})^{-1}(\theta - \alpha_t^{1/2}\mu_2). \quad (41)$$



## E Implementation details

All experiments are implemented with Python combined with PyTorch.

**Gaussian Mixture Model.** For sampling the posterior in the Gaussian Mixture Model, we consider the Metropolis-Adjusted Langevin Algorithm; see Roberts and Tweedie (1996). For a given number of observations  $n$ , we initialize the samples at  $n^{-1} \sum_{j=1}^n x_j^* + \epsilon$  where  $\epsilon \sim \mathcal{N}(0, \text{Id})$ . We run the MALA algorithm for  $10^3$  iterations with a learning rate of  $n^{-1} 10^{-3}$ . We adapt the learning rate in the first 500 iterations to target an acceptance ratio of 0.5. To do so, we increase the learning rate by a factor of 1.01 if the acceptance rate is larger than 0.5 or by a factor of 0.99 if the acceptance rate is smaller than 0.45.

**The score model.** Our implementation of the score model  $s_\phi(\theta, x, t)$  is an MLP with layer normalization and 3 hidden layers of respectively 128, 256 and 128 hidden features. It takes as input the embedded input variables  $(\theta, x, t)$  and outputs a vector of the same size as  $\theta \in \mathbb{R}^m$ . The embedding is done as follows:

- $\theta$  and  $x$  are each passed to an MLP with 3 hidden layers and 64 hidden features.
- A positional embedding is computed for  $t \in [0, 1]$  as per:  $(\cos(ti\pi), \sin(ti\pi))_{1 \leq i \leq F}$ , where we chose  $F = 32$  for the number of frequencies.

The score model is trained by minimizing the denoising score-matching (DSM) loss Song et al. (2020)  $\mathbb{E} [\|s_\phi(\theta, x, t) - \nabla_\theta \log q_{t|0}(\theta | \theta_0)\|^2]$ , parametrized with the VP-SDE and a linear noise schedule  $\beta(t) = 32t$ . For more stability we actually learn the *noise model*, which is related to the score model via  $\epsilon_\phi(\theta, x, t) = -\sigma(t)s_\phi(\theta, x, t)$ . Given a training dataset  $(\{(\theta_{0,i}, x_i)\}_{i=1}^{N_s} \sim p(\theta, x), t_i \sim \mathcal{U}(0, 1), z_i \sim \mathcal{N}(0, \mathbf{I}_m))$ , the empirical loss function writes:

$$\mathcal{L}(\phi) = \frac{1}{N_s} \sum_{i=1}^{N_s} \|\epsilon_\phi(\theta_i, x_i, t_i) - z_i\|^2, \quad \text{with } \theta_i = \sqrt{\alpha(t_i)}\theta_{0,i} + \sigma(t_i)z_i. \quad (42)$$

Note that for better training,  $\theta$  and  $x$  need to be normalized before being passed to the network (typically with the empirical mean and std of the training data).

All our models are trained over  $N_e = 5\,000$  epochs with early stopping based on the loss function computed on a held-out validation set (20% of the training set) and a learning rate of  $10^{-3}$  or  $10^{-4}$ , depending on which yields the best validation loss; see Appendix H. Empirically we observed that for large enough training sets ( $N_{\text{train}} > 10\,000$ ) early stopping is not necessary and not recommended, as no over fitting occurs and the score model needs to be trained as long as possible. In this case, the best model is selected after a minimum number of  $0.8 \times N_e$  epochs.

## F Additional results for the toy models

$m$	Speed up GAUSS	Speed up JAC
2	$0.39 \pm 0.01$	$0.56 \pm 0.00$
4	$0.39 \pm 0.01$	$0.55 \pm 0.00$
8	$0.39 \pm 0.01$	$0.56 \pm 0.00$
10	$0.38 \pm 0.01$	$0.52 \pm 0.00$
16	$0.38 \pm 0.01$	$0.54 \pm 0.00$
32	$0.37 \pm 0.01$	$0.52 \pm 0.00$

Table 2: Confidence intervals for the ratio between elapsed time for each algorithm (GAUSS, JAC) and the equivalent Langevin sampler in the Gaussian case for each tested  $m$ . The values are averaged over number of sampling steps,  $\epsilon$  and  $n$ .

Algorithm	N steps	$\Delta t$ (s)	$sW$
GAUSS	50	0.99 +/- 0.00	0.30 +/- 0.05
JAC	50	0.89 +/- 0.00	82.73 +/- 67.41
Langevin	50	1.77 +/- 0.01	0.24 +/- 0.01
GAUSS	150	1.83 +/- 0.01	0.31 +/- 0.04
JAC	150	2.66 +/- 0.00	5.89 +/- 1.07
Langevin	150	5.28 +/- 0.01	0.35 +/- 0.02
GAUSS	400	3.91 +/- 0.01	0.31 +/- 0.04
JAC	400	7.13 +/- 0.02	3.41 +/- 1.04
Langevin	400	14.06 +/- 0.04	0.43 +/- 0.02
GAUSS	1000	8.85 +/- 0.03	0.34 +/- 0.03
JAC	1000	17.69 +/- 0.07	7.33 +/- 5.41
Langevin	1000	35.08 +/- 0.15	0.47 +/- 0.02

Table 3: Sliced Wasserstein and total elapsed time for the Gaussian Mixture toy problem with  $d = 10$ ,  $n = 32$  and  $\epsilon = 10^{-2}$  per algorithm and number of generation steps. Mean and std over 5 different seeds.

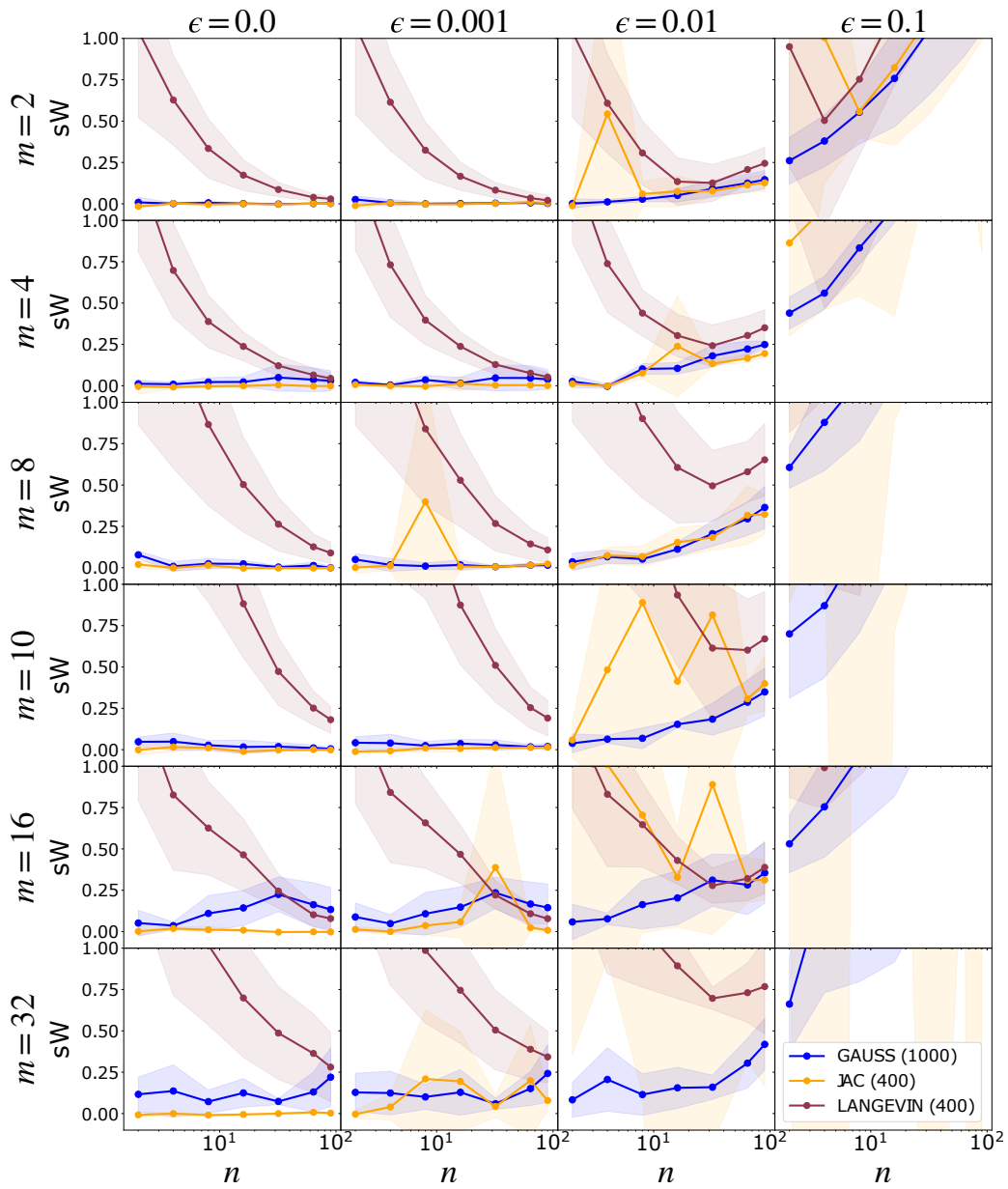


Figure 6: Normalized sW distance as a function of the number of observations  $n$  for **GAUSS**, **JAC** and **LANGEVIN** with different levels of  $\epsilon$ . Results are shown for the Gaussian example in several dimensions  $m \in [2, 4, 8, 10, 16, 32]$ . Mean and std over 5 different seeds.

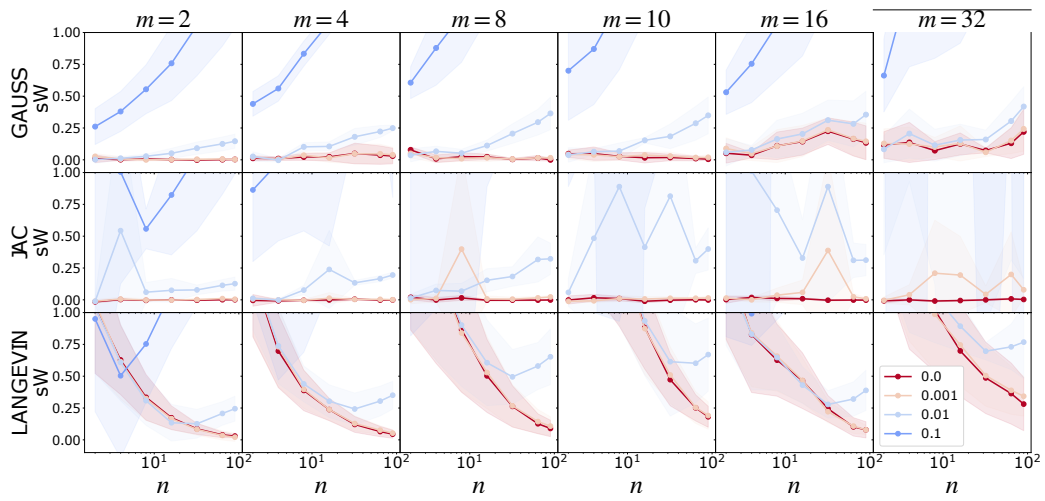


Figure 7: Sliced Wasserstein distance as a function of the number of observations  $n$  for the different methods with different levels of  $\epsilon$ . Results are shown for the Gaussian example in several dimensions  $m \in [2, 4, 8, 10, 16, 32]$ . Mean and std over 5 different seeds.

## G Additional results for SBI benchmarks

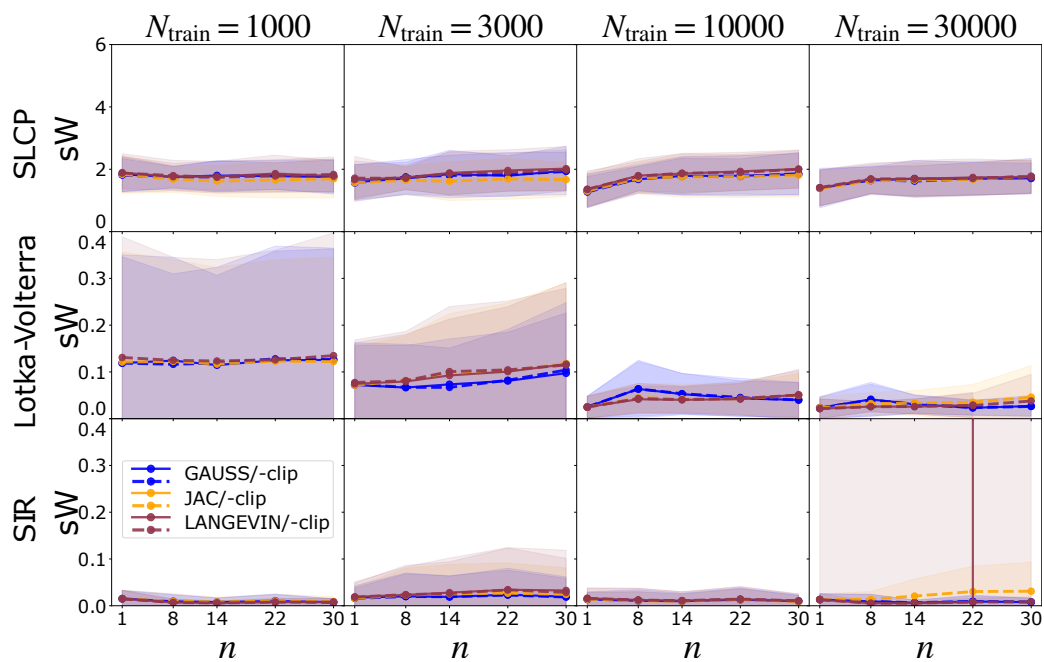


Figure 8: Sliced W2 a function of  $n \in [1, 8, 14, 22, 30]$  between the samples obtained by each algorithm and the true tall posterior distribution  $p(\theta \mid x_{1,n}^*)$  (for  $N_{\text{train}} \in [10^3, 3 \cdot 10^3, 10^4, 3 \cdot 10^4]$ ). Mean and std over 10 different parameters  $\theta^* \sim \lambda(\theta)$ .

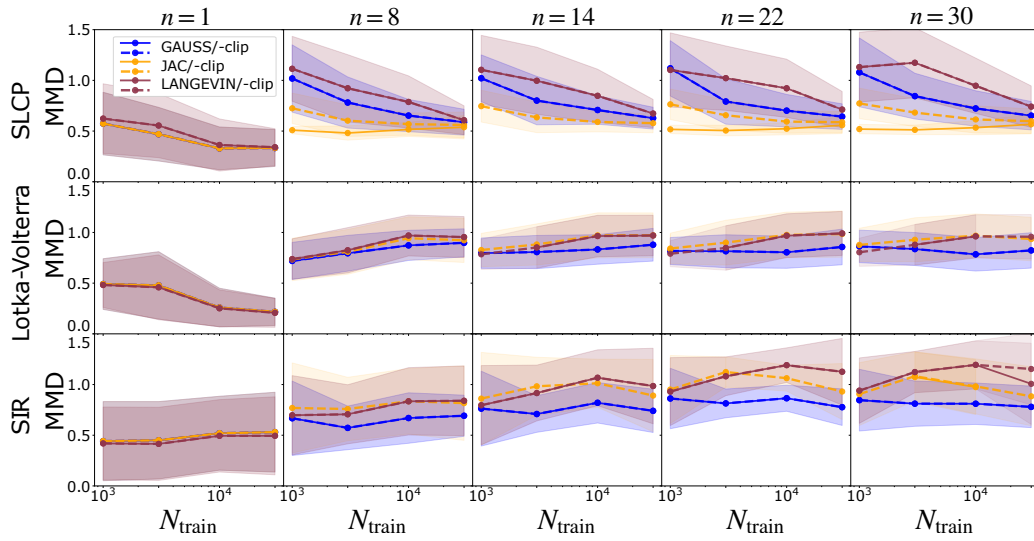


Figure 9: MMD as a function of  $N_{\text{train}} \in [10^3, 3.10^3, 10^4, 3.10^4]$  between the samples obtained by each algorithm and the true tall posterior distribution  $p(\theta \mid x_{1,n}^*)$  (for  $n \in [1, 8, 14, 22, 30]$ ). Mean and std over 10 different parameters  $\theta^* \sim \lambda(\theta)$ .

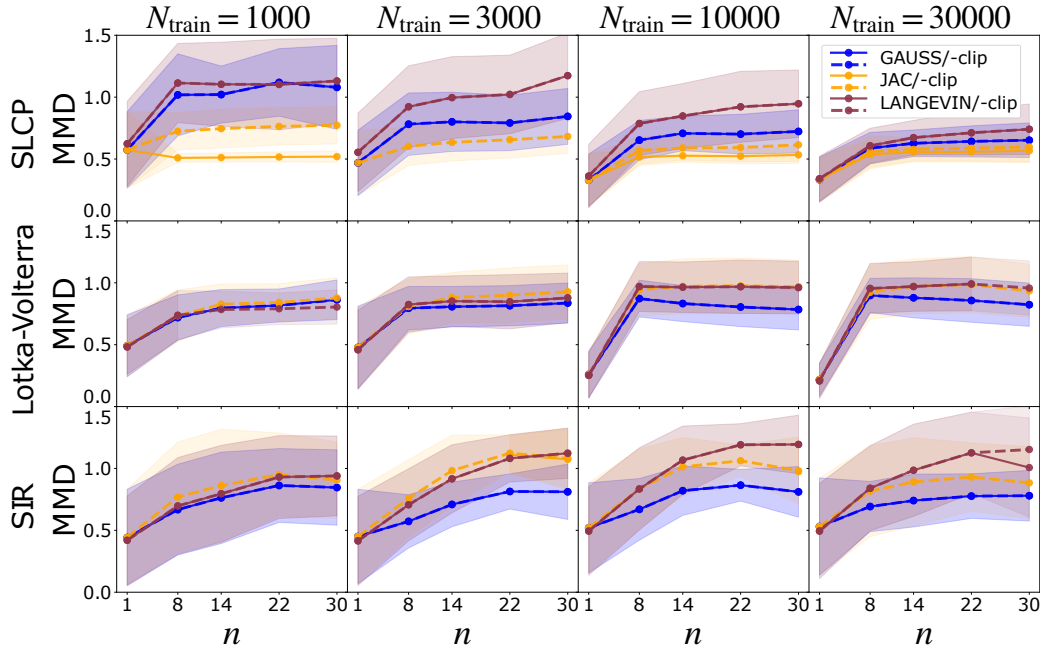


Figure 10: MMD as a function of  $n \in [1, 8, 14, 22, 30]$  between the samples obtained by each algorithm and the true tall posterior distribution  $p(\theta \mid x_{1,n}^*)$  (for  $N_{\text{train}} \in [10^3, 3.10^3, 10^4, 3.10^4]$ ). Mean and std over 10 different parameters  $\theta^* \sim \lambda(\theta)$ .

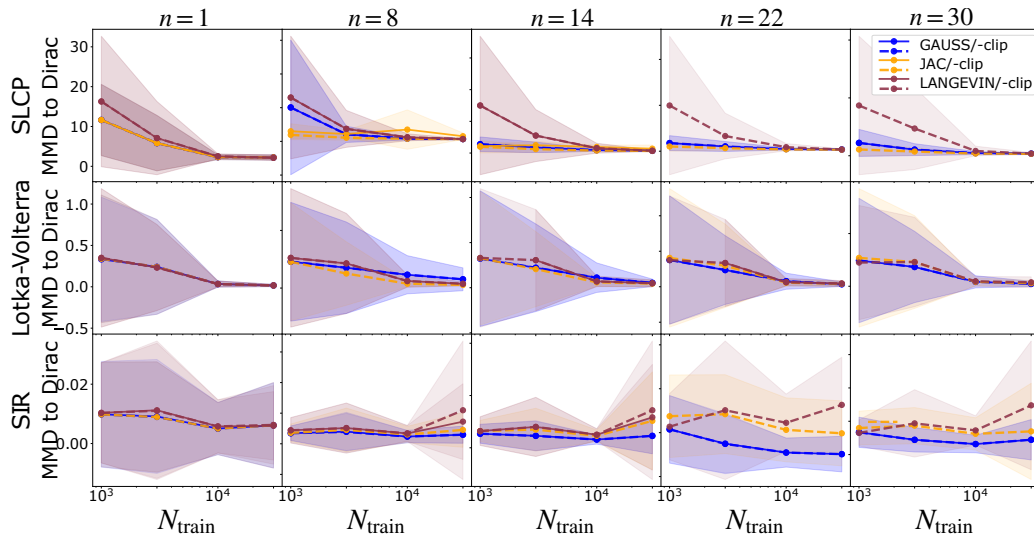


Figure 11: MMD as a function of  $N_{\text{train}} \in [10^3, 3.10^3, 10^4, 3.10^4]$  between the marginals of the approximate tall posterior distribution  $p(\theta | x_{1,n}^*)$  and the Dirac of the true parameters  $\theta^*$  used to simulate the observations  $x_{1,n}^*$  (for  $n \in [1, 8, 14, 22, 30]$ ). Mean and std over 10 different parameters  $\theta^* \sim \lambda(\theta)$ . The concentration around the true parameter generally increases (decreasing MMD) with  $N_{\text{train}}$ , i.e. the estimation of the posterior distribution is more precise.

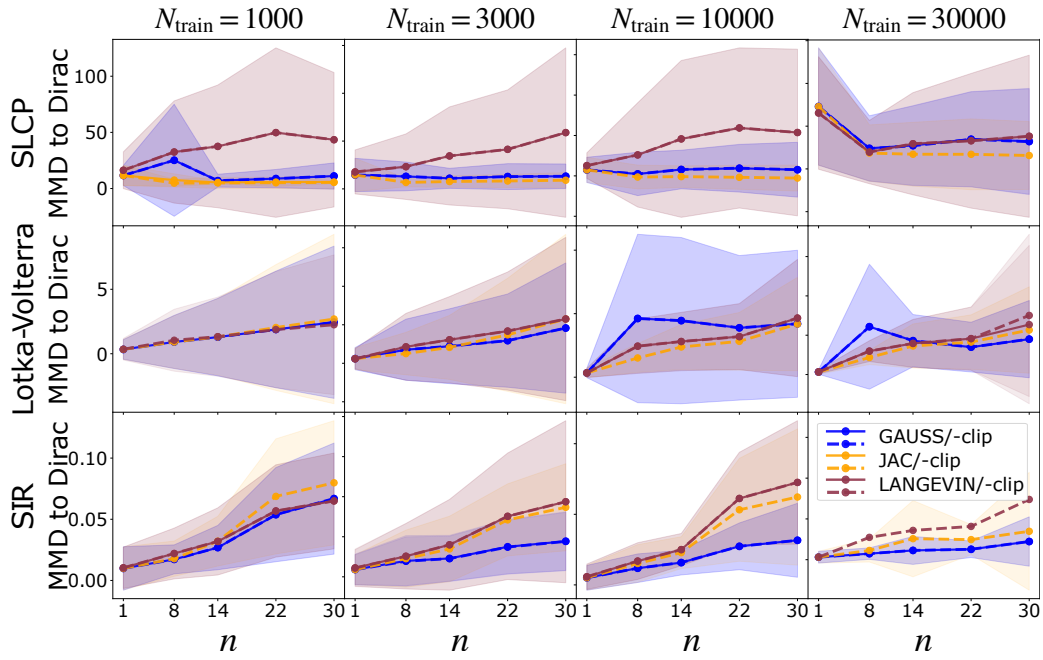


Figure 12: MMD as a function of  $n \in [1, 8, 14, 22, 30]$  between the marginals of the approximate tall posterior  $p(\theta \mid x_{1,n}^*)$  (for  $N_{\text{train}} \in [10^3, 3 \cdot 10^3, 10^4, 3 \cdot 10^4]$ ) and the Dirac of the true parameters  $\theta^*$  used to simulate the observations  $x_{1,n}^*$ . Mean and std over 10 different parameters  $\theta^* \sim \lambda(\theta)$ .



## H Loss functions

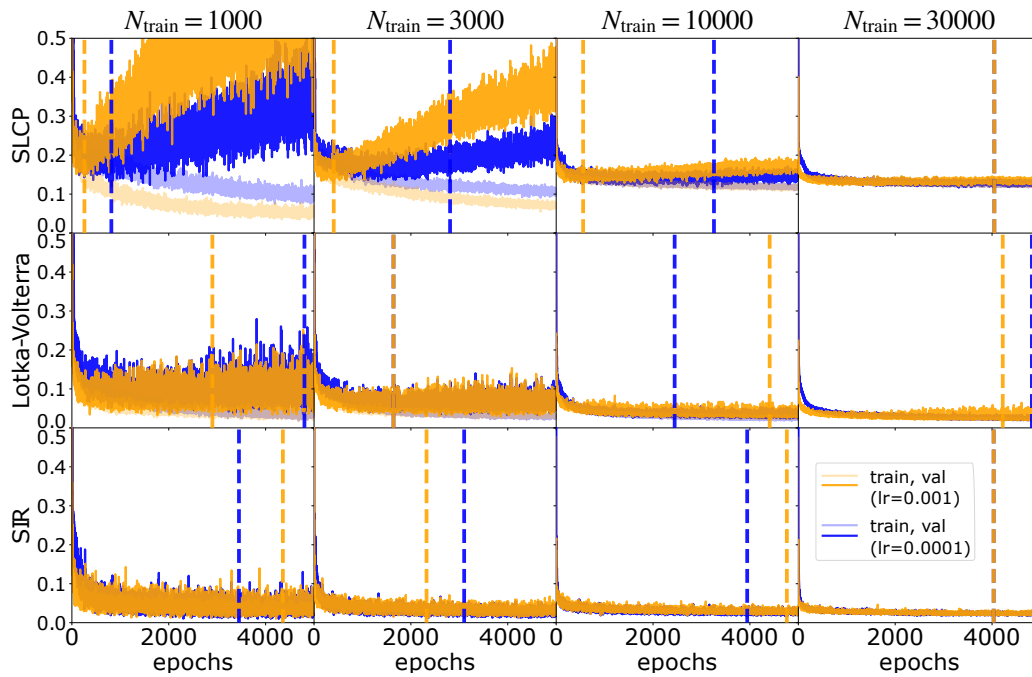


Figure 13: Loss functions for the SBI benchmark examples. The validation loss was computed on a held-out validation set of 20% of the training dataset. Dotted lines indicate the epoch at early stopping time.. Results are shown for  $N_{\text{train}} \in [10^3, 3 \cdot 10^3, 10^4, 3 \cdot 10^4]$ . The score networks were chosen according to the learning rate yielding the best validation loss (here always  $10e^{-4}$ , except for Lotka Volterra with  $N_{\text{train}} = 3 \cdot 10^4$ ).

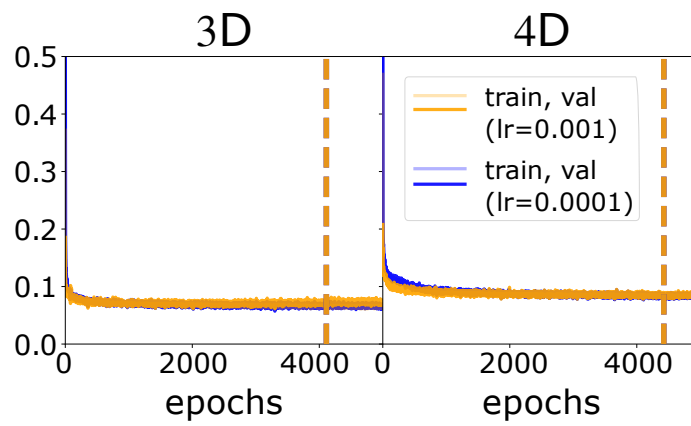


Figure 14: Loss functions for the Jansen & Rit Neural Mass Model. The validation loss was computed on a held-out validation set of 20% of the training dataset of size  $N_{\text{train}} = 50\,000$ . Dotted lines indicate the epoch at early stopping time. The score network was chosen according to the learning rate yielding the best validation loss (here always  $10e^{-4}$ ).